Analytical Chemistry
Volume 97, Issue 42, October 2025, pp. 23496-23504
DOI:10.1021/acs.analchem.5c04753

A Tandem Cubic DNA Nanostructures Cell Membrane Surface Sensing Platform for in situ Monitoring of Multiple Cytotoxicity Related Biomarkers

Jin Wang[1], Zhugen Yang[2], Kun Wang[3], Zhen Zhang[1]*

[1]School of the Environment and Safety Engineering, Jiangsu University, Zhenjiang 212013, China

[2]School of Water, Energy, and Environment, Cranfield University, Cranfield MK43 0AL, UK

[3]The School of Chemistry and Chemical Engineering, Jiangsu University, Zhenjiang 212013, China

*Corresponding author:

Email: zhangzhen@ujs.edu.cn (Zhen Zhang)

ABSTRACT: Emerging organic pollutants (EOPs) are considered to exhibit extensive toxicity to human bodies. However, monitoring of this toxicological process is hampered by the shortage of suitable methods to track endogenous biochemical factors under living cell level. To solve this technical challenge, a cell surface fluorescent sensing platform using tandem cubic DNA nanostructures (tCDNs) as the main architectures is developed in this work. With the precise assembly of several prefabricated DNA wireframe modules, a set of linear nano-superstructures can be efficiently hydrophobic anchored to the cell membrane surface. Furthermore, two different aptamer-based fluorescence recognition elements targeting adenosine triphosphate (ATP) and dopamine (DA) can be modified on top of tCDNs in an equidistant arrangement, serving as a core part for monitoring endogenous cellular biochemical factors. As a typical example, we used tetrabromobisphenol A bis(2-hydroxyethyl ether) (TBBPA-BHEE) induced living cells as a toxic effect system to monitor the release of endogenous ATP and DA in a direct visualization manner. On this basis, the correlation between the concentrations of these two endogenous biochemical factors (ATP and DA) and different TBBPA-BHEE exposure conditions were explored. We believe this work can provide a robust and promising tool for studying the cellular toxicological mechanisms caused by pollutants.

Keywords: Cytotoxic monitoring, Cell membrane probes, Cellular imaging, Biomarkers, DNA nanotechnology

Published by ACS. This is the Author Accepted Manuscript issued with: Creative Commons Attribution License (CC:BY 4.0).
The final published version (version of record) is available online at DOI:10.1021/acs.analchem.5c04753. Please refer to any applicable publisher terms of use.

INTRODUCTION

The health concerns arising from emerging organic pollutants (EOPs) via their induced damage to human cells have attracted growing attention.[1-3] For example, tetrabromobisphenol A bis(2-hydroxyethyl ether) (TBBPA-BHEE), the most water-soluble derivative of tetrabromobisphenol A (TBBPA), has been reported to exhibit significant toxicity toward both cellular systems and whole organisms.[4-6] Given the complexity of the damage situation to human cells by these organic contaminants, the method to monitor such toxicological process holistically is critical for understanding the mechanism of pollutant toxicity effects.[7, 8] With this in mind, numerous analytical techniques have been developed to monitor cellular biochemical parameters, aiming to identify critical evidence of pollutant-induced biological damage. For instance, kits for detecting the activity of intracellular factors (such as acetylcholinesterase, lactate dehydrogenase, glutathione, etc.),[9-11] real-time quantitative PCR methods for determining RNA levels and western blot technology for measuring target proteins.[12-14] However, these static endpoint damage assessment methods cannot be applied to tracking of the microscopic process of pollutant-induced cytotoxic effects.[15-17] Therefore, it is highly desirable to find a non-destructive in situ living cell monitoring method to track the changes of cellular endogenous factors.

As a reliable and non-invasive approach for monitoring endogenous biochemical indicators, nucleic acid nanomaterial-based cell membrane surface functionalization strategies have recently emerged garnered increasing attention due to the high

programmability of DNA sequences derived from accurate Watson-Crick base-pairing properties.[18, 19] Combined with high affinity and specificity aptamer recognition elements, researchers have developed a variety of DNA-based cell membrane surface aptamer biosensors to target different biochemical factors, such as adenosine triphosphate (ATP), dopamine (DA), H^+, and metal ions.[20, 21] These cell-surface-anchored strategies have been demonstrated to be well-performing methods for analyzing extracellular microenvironment biomarkers.[22, 23] Nevertheless, DNA biosensors based on existing cell membrane surface functionalization technologies are still insufficient to meet the requirements of pollutant cytotoxicity monitoring due to two technical bottlenecks.

On the one hand, so far, there is no cell membrane surface anchoring strategy that can balance robustness, versatility, and ease of operation.[24-26] For example, the firm covalent modification method is often accompanied by tedious technical steps, the easy-to-use hydrophobic insertion method is not stable enough, while the specific binding strategy using recognition molecules are usually lacks versatility.[27-29] In addition, most of these modification methods will damage cell activity, thereby affecting the accuracy of the final measured parameters.[30] Another challenge lies in the reported cell membrane surface sensors usually only target a single biomarker, since the designed DNA nano-substrate structure is too simplistic to load a variety of recognition elements.[31-33] Although Amphiphilic 3D DNA origami has been proven to provide abundant binding sites, but apparently, the high synthesis cost and excessive

structural rigidity mean that it is not suitable for becoming a universal sensing platform.[34, 35]

In response to the above considerations, we describe here strategies to rationally engineer a tandem cubic DNA nanostructures (tCDNs) as the main architecture of the living cell surface microenvironment sensing platform. With a simple hierarchical construction approach, DNA cube monomers are connected in series by a specially designed wireframe structure, thus easily achieving a firm and flexible wrapping of the cell membrane surface. Four cholesterol molecules at the bottom of each DNA cube inserted in the middle of the cell membrane lipid bilayer with consistent directionality and appropriate density, providing strong adhesion for the DNA materials. In addition, the exchange of substances between cells and the external solution can be achieved by the space reserved between linear semi-encapsulation configurations and nanopores inside the tandem DNA frameworks. Combining excellent target recognition capability and high diversity of the DNA aptamer probes, a stable and efficient in situ sensing platform for extracellular biochemical factors (ATP and DA) was established. Furthermore, based on this strategy, the toxicity mechanism of new organic pollutants was explored using TBBPA-BHEE induced living cells as a model.

MATERIALS AND METHODS

The required materials and instruments are provided in the Supporting Information.

Construction of the tandem cubic DNA nanostructures (tCDNs). TCDNs are formed by a three-step assembly process. The first step is the preparation of DNA cubes. Briefly, the four oligonucleotide strands (C1-4 for DNA cube 1 or C5-8 for DNA cube 2 in Table S1, 1 μL, 100 μM) that constitute the main structure of the DNA cube were mixed in TAM buffer (40 mM Tris, 12.5 mM Mg^{2+}, 1 mM EDTA, 20 mM acetic acid, pH=7.4) at a molar ratio of 1:1:1:1 to a final volume of 50 μL, followed by the annealing protocol using an automated polymerase chain reaction (PCR) thermal cycler: 95 °C, 5 min; 85 °C, 5 min; the temperature was slowly lowered to 60 °C at a rate of 2 min/°C, and then slowly lowered to 4 °C at a rate of 3 min/°C. In the second step, after the main framework of the DNA cube was formed, cholesterol-modified short strands (CT20, 4 μL, 100 μM) were added into the solution system and incubated at 37 °C for 2 h to complete the hydrophobic molecular functionalization of the DNA cube monomer. Finally, the prepared DNA cube 1 and 2 were mixed in equal amounts, and the long oligonucleotide strands L1 and L2 of the same concentration were added and incubated at 37°C for 20 min to form tCDNs.

Preparation of tCDNs nanosensing platform. When tCDNs are prepared, the connection of the aptamer fluorescent recognition element is completed using the DNA long strands L50-1 and L50-2 as a link. In particular, the fluorescent recognition elements based on adenosine triphosphate (ATP) and dopamine (DA) aptamers were self-assembled from the corresponding functional DNA strands (A1-3 for ATP, DP and CP for DA) through a programmed heating-annealing process (heated at 95 °C for

5 min and then naturally cooled to room temperature). The two aptamer recognition elements were mixed with the corresponding linker long strands (L50-1 and L50-2) in a molecular ratio of 1:1, and then added to the tCDNs solution system and incubated at 37°C for 30 min to complete the assembly of the nanosensing platform.

Cell culture. CCRF-CEM cells were cultured in 1640 medium supplemented with 10% FBS and 100 U/mL of penicillin-streptomycin (10000 IU penicillin and 10000 μg/mL streptomycin). SH-SY5Y cells were grown in MEM/F12 medium (1:1) containing 10% FBS and 100 U/mL of penicillin-streptomycin. All cells were cultured at 37 ℃ in a humidified atmosphere incubator containing 5% CO_2. In addition, SH-SY5Y cells were digested by trypsinization with 0.1% trypsin (0.02% EDTA, 0.05% dextrose, and 0.1% trypsin) in phosphine-buffered saline (PBS, pH=7.2). Hemocytometer is used for cell density statistics before any experiment.

Imaging of the tCDNs on the cell surface. 1×10^5 CCRF-CEM cells were washed three times with 1× PBS buffer and then added cholesterol-labeled DNA cubes 1 and 2 to make them immobilized on membrane surface. Subsequently, the long oligonucleotide strands (L1 and L2) and the aptamer-based fluorescence recognition elements are introduced step by step to fabricate the tCDNs on cell surface by shaking cells at 240 rpm for 10 minutes. All assembly experiments were carried out in cell culture medium without serum. The samples were imaged by confocal microscopy without further treatment.

Imaging of exogenous ATP and DA on the cell surface. SH-SY5Y cells were

seeded in a 35 mm confocal glass-bottom dishes and incubated with MEM/F12 medium (1:1) containing 10% FBS at 37 °C to reach 80% confluency. Then, the medium was removed, and the cells were washed with 1× PBS three times. After that, the cells were incubated with MEM/F12 medium (1:1) containing different concentrations of TBBPA-BHEE for specific duration. Finally, the cells were modified with tCDNs using the above method and imaged by confocal microscopy without further treatment.

RESULTS AND DISCUSSION

Design of the tCDNs sensing platform. To construct the cell membrane surface sensing platform based on tCDNs, two sets of oligonucleotide sequences and connecting wireframes for assembling DNA cubes were designed (Table S1 and Figure S1). Among them, the scaffold DNA strands (C1-C4 and C5-C8) were precisely self-assembled in an end-to-end manner after a programmed heating-annealing process to generate the main framework of DNA cube 1 and 2. By utilizing a cholesterol-labelled DNA strand (CT20), DNA cube monomers could be immobilized on the cell membrane surface by means of the hydrophobic insertion between cholesterol molecules and lipid bilayer. Subsequently, based on the principle of base complementary pairing, the DNA wireframes L1 and L2 laterally connected the two DNA cube monomers into a tandem nanostructure, greatly enhancing the anchoring stability of the nucleic acid framework material. Once the DNA

superstructure base is fully established, the aptamer fluorescent elements targeting two endogenous cell markers (ATP and DA) will be longitudinally connected to the top of the tandem framework structure with the help of pre-designed DNA sequences (L50-1 and L50-2). Relying on the excellent addressability of DNA materials, the two DNA aptamer elements will be arranged in order on the two side tracks of the tandem architectures.

Scheme 1 depicts the fluorescence imaging mechanism of ATP and DA after the cell membrane surface sensing platform was completely constructed. In short, the aptamer's good specific recognition ability for the target triggers the dynamic changes of the DNA conformation at the microscale, which ultimately leads to two different fluorescence signal response modes and imaging strategies. For ATP, in situ fluorescence imaging was achieved by well-designed nano-switch, a DNA nano-tweezer with split ATP aptamers connected to the ends of both arms, composed of three ssDNA stands. The DNA tweezer structure was closed due to the specific capture of endogenous ATP by the split aptamers, bringing the fluorescent donor (Cy3, λ_{ex}=550 nm, λ_{em}=570 nm) and acceptor fluorophores (Cy5, λ_{ex}=650 nm, λ_{em}=670 nm, Figure S2) close to each other, and then a high fluorescence resonance energy transfer (FRET) ratio can be read out. On the other hand, for the detection of DA, a double-stranded complex with a fluorophore (FAM, λ_{ex}=495 nm, λ_{em}=520 nm) and a quencher (BHQ-1) were proposed. In the absence of DA, the intact duplex allows BHQ-1 to be close enough to quench the fluorescence of FAM. When DA is

present in the cell membrane surface fluid microenvironment, the high-affinity aptamer (DP) will recognize and capture DA molecule, thereby triggering the separation of the complementary strand CP with a quencher, and ultimately the FAM fluorescence signal will be restored. The fluorescence changes induced by ATP and dopamine (DA) at the cell membrane surface will be captured by confocal laser scanning microscopy (CLSM), with quantification of target molecule concentrations derived from grayscale analysis of CLSM images. In summary, the monitoring of ATP and DA targets were well executed through the rational construction of two DNA aptamer recognition elements.

Fabrication of tCDNs and DNA aptamer recognition elements. Firstly, after verifying the integrity of DNA cube backbone DNA oligonucleotides (C1-C8) and auxiliary DNA strands (L1, L2, L50-1, L50-2 and CT20) by 12% native polyacrylamide gel electrophoresis (Figure S3 and S4), we used agarose gel electrophoresis to investigate the generation of DNA cube monomers. In Figure 1A, the hierarchical self-assembly of the DNA cube framework via accurate Watson-Crick base pairing was verified by the sample bands with gradually slower migration rates. Until all four backbone DNA oligonucleotides (C1-C4 or C5-C8) were added, the main structure of the DNA monomer cube was completely assembled (Lane 4 in Panel Ⅰ and Ⅱ). Furthermore, each unit of DNA cube can combine with 4 units of cholesterol-modified short strand CT20 and two types of bridge single strands (L50-1

and L50-2) each 1 unit to form a functional monomer structure (Lane 5, 6 in Panel Ⅰ and Ⅱ).

In the next step, the assembly of tandem cubic DNA nanostructures was demonstrated by 12% native polyacrylamide gel electrophoresis (Figure 1B). After the assembly process described above was achieved, complete and clear electrophoresis bands were presented (Lane 1 for DNA cube 1 and Lane 2 for DNA cube 2). Subsequently, with the assistance of the DNA wireframes L1 and L2, DNA cubes 1 and 2 are arranged in an orderly manner at intervals to form tCDNs. Correspondingly, on electrophoresis track Lane 3, a prominent dark band with a significantly slower migration rate is presented, indicating the generation of macromolecular DNA polymers. These electrophoresis results confirmed that the DNA cubes and their higher-order structures, tCDNs, did indeed form as design. In addition, the atomic force microscope (AFM) image demonstrated the morphology and size of these DNA cubes (Figure S5A) and their assembled tCDNs (Figure S5B).

In particular, the successfully assembled tCDNs should be further validated for stability under complex solution conditions. For this purpose, distinct solution conditions were designed to test the anti-degradation ability of tCDNs. As seen in Figure S6A and B, tCDNs were incubated for 2-10 hours under conditions of 0.5 U/mL DNase I and 10% FBS, respectively. Subsequent electrophoresis results demonstrated that the tCDNs maintained their superstructure conformation under both challenging conditions. In like manner, the electrophoresis results of tCDNs after

incubation at pH 5-9 for 10 hours confirmed that it has robust acid-base resistance (Figure S6C).

Beyond that, the formation of the ATP and DA aptamer fluorescence nano-switch were also verified by using agarose gel electrophoresis. Figure S7A illustrates the assembly details of the ATP-aptamer-based nano-tweezers. Correspondingly, as shown in Figure S7B, Lanes 1, 2 and 3 represent the A1, A2 and A3 strands, respectively. Among them, split ATP aptamers were integrated at the end of A1 and A2 strands, while Cy3 and Cy5 fluorophores were attached to both ends of the A3 DNA strand. When these three DNA strands are assembled in equal molar amounts and ultimately form the composite DNA nano-tweezer structures, the movement rate of electrophoretic bands gradually slows down due to the increase in hybridization complex molecular weight (Lanes 4 and 5). Similarly, the assembly of DA aptamer recognition element based on the design of Figure S8A has also been confirmed, attributed to the slow-moving bands exhibited by the DP/CP double strand composite structures (Lane 3 in Figure S8B).

In vitro detection of ATP and DA. After the assembly of all the main structures of tCDNs and the corresponding aptamer elements were verified, as a prerequisite for in situ monitoring of biomarkers on the cell membrane surface, we first investigated the in vitro detection performance of the proposed sensing platform for ATP and DA. For ATP sensing, as illustrated in Figure 2A, the presence of ATP molecules induces the activation of DNA nano-switches and causes the split ATP

aptamers located at the ends of A1 and A2 to approach each other, thereby triggering the FRET between the fluorescent acceptor (Cy5) and donor (Cy3). Within the molecular concentration range of the target substance from 0 to 500 μM, the FRET effect enhanced with the increase of ATP concentration leads to the weakening of Cy3 fluorescence and the strengthening of Cy5 fluorescence (Figure 2B and C). Moreover, the data in Figure 2D showed a good linear relationship between ATP concentrations (0-60 μM) and Cy3/Cy5 fluorescence signal ratio with the limit of detection (LOD) of 0.96 μM (S/N=3, R^2=0.998). Notably, the detection range and sensitivity of ATP fluorescence aptamer recognition element exhibits excellent compatibility with the extracellular ATP concentration levels reported in the literature, which provides a crucial prerequisite for establishing cell membrane surface sensing platforms.[36-38] Furthermore, the selectivity of the ATP aptamer element was also revealed through control experiments (see Figure S9 and accompanying discussion for details) using ATP analogs including GTP, UTP, and CTP at equivalent concentrations as reference substances.

For the in vitro concentration analysis of DA, the key mechanism enabling FAM fluorescence recovery relies on the high-affinity binding between DA molecules and their aptamer, which triggers the dissociation of the quencher (BHQ-1) labeled complementary DNA strands (Figure 3A and S10). As the DA concentration increased from 0 to 100 μM, progressively higher FAM fluorescence intensity can be read out, and a good linear relationship was observed in the range of 0-2000 nM

(Figure 3B, C and D). Meanwhile, according to these results, the LOD was calculated to be 0.62 nM. In addition, to investigate the specificity of the aptamer sensing element to DA, a set of homologs was co-incubated with the aptamer complex and confirmed that only the solution system containing DA molecules could effectively induce the recovery of FAM fluorescence (see Figure S11). Taken together, the above results demonstrate that the fabricated sensing platform exhibits satisfactory performance for in vitro detection of ATP and DA, providing a convincing foundation for further construction of cell membrane fluorescence imaging systems.

The validation of cell-surface anchoring and biocompatibility of tCDNs. Motivated by the above results, we subsequently investigated the cell-surface anchoring capability of tCDNs. As an exemplary suspension cell model, CCRF-CEM cells—a human acute lymphoblastic leukemia (ALL) cell line—were employed in this series of studies. Besides this, to achieve efficient fluorescent labeling, a Cy3-modified DNA strand (LF) was assembled onto the tCDNs, replacing the original aptamer elements. After co-incubation with the specifically designed tCDNs, CCRF-CEM cells were treated with the DiO cell membrane staining kit according to the standardized protocol for 20 minutes. In parallel, as a control group, CCRF-CEM cells were co-incubated with tCDNs lacking the hydrophobic DNA strand (cholesterol-modified short strand, CT20) following identical experimental procedures. The experimental results are clearly presented by

CLSM in Figure S12: Cy3 fluorescence signal exhibits precise colocalization with the green fluorescence from DiO membrane dye, confirming efficient tCDN membrane anchoring through their properly aligned and uniformly oriented cholesterol modifications. In contrast, tCDNs lacking the CT20 DNA strand exhibited negligible Cy3 fluorescence in cells, further demonstrating that the amphiphilic affinity conferred by cholesterol moieties is essential for the membrane-surface modification of DNA architectures.

To enable effective monitoring of target molecules in cell membrane microenvironment, an optimal DNA nanomaterial superstructure platform should exhibit stable single-cell surface anchoring while preventing intercellular transfer between adjacent cells. This is also one of the important goals that our proposed tandem framework superstructure should achieve. Accordingly, two groups of CCRF-CEM cells were separately modified with either monomeric DNA cubes or tCDNs (Figure S13), then each mixed with an equal number of nuclear-labeled cells (stained with Hoechst 33342 dye) for one hour incubation. As shown in Figure 4A, after one hour of homogeneous mixing with Hoechst 33342-labeled cells, approximately 23% of DNA cube monomers-modified cells exhibited Cy3 fluorescence transfer, indicating insufficient anchoring stability of these isolated DNA framework structures on the cell membrane surface (Panel Ⅰ). As a striking contrast, the CLSM images in Panel Ⅱ show no cells simultaneously labeled with both Cy3 and Hoechst 33342, demonstrating that tCDNs-modified cells exhibit

remarkable stability which effectively prevents intercellular fluorescence crosstalk. The effectiveness of tCDNs anchoring were further confirmed by Figure 4B, compared to Panel II, Panel I demonstrated a distinct fluorescence spatial distribution pattern: Cy3 fluorescence was predominantly localized at the cell periphery along the line segment, while Hoechst 33342-derived blue fluorescence was centrally positioned.

The maintenance time of tCDNs architecture on the cell membrane surface is another important performance indicator due to the performance requirements of long-time monitoring of target substances in the intercellular microenvironment. CLSM images in Figure S14A and B present comparative experimental results between monomeric DNA cubes and tCDNs after 0-6 hours co-incubated with CCRF-CEM cell lines. After a 3-hour incubation period, the Cy3 fluorescence used to label DNA cube monomers exhibited significant attenuation on the cell membrane, indicating the detachment or disintegration of the monomeric DNA framework. In contrast, cells modified with tCDNs maintained stable fluorescence persistence for at least 6 hours, providing direct evidence of the remarkable structural robustness originating from this rationally engineered architecture. Collectively, these experimental results robustly demonstrate the successful achievement of a key developmental objective of tCDNs—significantly enhancing the anchoring stability of DNA framework structures on cell membranes—thereby providing an important prerequisite for the final establishment of fluorescence sensing platform.

Furthermore, in contrast to membrane coating achieved through DNA origami or DNA strand amplification techniques,[39-41] tCDNs exhibit another distinct advantage by maintaining normal cellular physiological functions post-modification. In this regard, we employed two distinct strategies to investigate the survival status of cells modified with tCDNs. First, the standard CCK-8 assay was employed to measure cell viability at three different tCDNs concentrations (calculated based on the concentration of DNA cube monomers contained) after varying incubation periods. As illustrated in Figure 5A, the cells maintained satisfactory viability under all tested conditions. Even after 48 hours incubation at the highest concentration (200 nM), the cells were able to maintain a survival rate of no less than 88.6%. Furthermore, the survival status of individual cells was observed after using the Calcein-AM living cells fluorescence dye kit. Following cellular uptake, Calcein-AM is hydrolyzed by intracellular esterases to yield Calcein, a polyanionic dye that exhibits intense green fluorescence. As evidenced by Figure 5B and C, all CCRF-CEM cells within the CLSM field of view exhibited dual fluorescence labeling (red: Cy3; green: Calcein) with a distinct outer-to-inner distribution pattern following treatment with tCDNs-modified DNA nanostructures and the Calcein-AM dye kit. These results collectively demonstrate that the cells maintained high viability while being efficiently functionalized by the DNA nanostructures, which can be attributed to two key factors: (1) Compared to dense mesh-like coatings, the linear arrangement of tCDNs preserves sufficient exposed membrane surface area; and (2) The uniformly

porous architecture of tCDNs, enabled by monomeric DNA cubes, ensures unimpeded exchange of metabolites between cells and their microenvironment.

In situ imaging of exogenous ATP and DA on the cell membrane surface. To demonstrate the feasibility of dual-target imaging on the cell membrane surface using an in situ-anchored tCDNs-based fluorescent sensing platform, we engineered tCDNs assemblies loaded with fluorescent aptamers and achieved their stepwise conjugation on the surface of SH-SY5Y cells (a model human neuroblastoma cells). Subsequently, cells were incubated with PBS buffer containing different concentrations of exogenous targets and subjected to CLSM imaging. As shown in Figure S15A, the merged graph of red channel (Cy3) and purple channel (Cy5) exhibited a significant grayscale variation along with the change of the ATP concentration. When there are no exogenous ATP molecules present in the extracellular microenvironment, prominent red fluorescence was observed, while minimal purple fluorescence was detected, indicating that almost no FRET effect occurs due to the sufficient distance between the Cy3 and Cy5 fluorescent groups on the DNA aptamer nano-tweezers. With increasing concentrations of exogenous ATP, progressively enhanced FRET efficiency was observed, characterized by diminishing red fluorescence (Cy3) and intensifying purple fluorescence (Cy5), due to ATP-induced proximity of the split aptamer on the DNA recognition element. Moreover, ImageJ software was used to analyze the fluorescence profiles of the middle cross-section in living cells. The fluorescence intensity curve obtained after

removing the background (Figure S15C, Panel I) demonstrated a concentration-dependent increase in the Cy5/Cy3 fluorescence ratio with rising ATP levels, consistent with the results presented in Figure 2. These findings further validate that the proposed tCDNs fluorescent sensing platform can effectively in situ respond to ATP in cellular membrane microenvironments.

Furthermore, exogenous DA molecules of different concentrations (0-50 μM) were added to the cell membrane surface microenvironment to test the response of the fluorescence sensing platform to DA. As expected, with the competitive effects caused by an increasing number of DA molecules, increasingly significant FAM fluorescence recovery was presented (Figure S15B). In Figure S15C Panel II, the average fluorescence intensity analysis along the yellow line of this green channel further processed by the ImageJ software (background removed) is in accordance with Figure 3. These data showed that the fluorescence imaging of FAM displayed a significant DA-dependent signal. In summary, the fluorescence imaging results from three distinct channels (Cy3, Cy5 and FAM) collectively demonstrate that the proposed tCDNs sensing platform enables efficient in situ monitoring of exogenous targets (ATP and DA) in the cell membrane surface microenvironment.

Specifically, to validate the universality of the proposed tCDNs-based fluorescent sensing platform across different cell types and to exclude potential signal crosstalk between FAM and Cy3/Cy5 fluorophores, CCRF-CEM cells modified with tCDNs fluorescent sensing structures were co-incubated with 100 μM

ATP and 50 μM DA. As illustrated in Figure S16A and B, the two target molecules independently triggered Cy3/Cy5 FRET fluorescence signal changes and FAM fluorescence recovery, respectively, demonstrating the capability of the established sensing system to monitor the two analytes independently. Furthermore, the tCDNs cell membrane-anchoring system constructed with mismatched aptamer sequences failed to elicit the corresponding fluorescence response upon target binding (Figure S16C), confirming the excellent specificity of the tCDNs sensing system for monitoring cell membrane surface targets.

In situ monitoring of endogenous ATP and DA in TBBPA-BHEE induced SH-SY5Y cells. As a class of emerging organic pollutants, TBBPA and its derivatives have been reported to exhibit significant neurotoxicity and are attracting increasing concern due to their widespread applications.[42-44] Among these, TBBPA-BHEE exhibits the highest toxicity due to its water solubility and disrupts secretion of many biochemical markers (e.g., ATP and DA) in neural cell model.[4, 45] However, traditional methods only provide static, macroscopic, and non-real-time assessments of cellular damage, failing to capture the microscopic progression of pollutant-induced cytotoxic effects. Therefore, as the ultimate and most critical objective, the proposed tCDNs sensing platform in this study is designed to enable in situ monitoring of endogenous biomarkers in cellular models exposed to TBBPA-BHEE, thereby achieving in depth assessment of pollutant-induced cytotoxicity. For this purpose, we initially exposed SH-SY5Y cells to various concentrations of TBBPA-

BHEE (0-30 μM) for 24 hours to establish an appropriate cellular model, followed by monitoring endogenous biochemical markers using tCDNs-based fluorescent sensing platform according to above validated protocol. As shown in Figure 6A, the Cy5/Cy3 fluorescence ratio exhibited a concentration-dependent increase with elevated TBBPA-BHEE levels, indicating progressively higher concentrations of endogenously secreted ATP in the cell membrane microenvironment. In striking contrast, the green fluorescence signal (FAM) manifested a unique kinetic profile featuring an initial decline followed by a subsequent rebound, which faithfully reflected the V-shaped concentration-dependent secretion pattern of endogenous dopamine (DA). Based on these findings, some conclusions can be drawn: (i) Low-dose TBBPA-BHEE (10 μM) exhibits neurotoxic effects, as evidenced by reduced DA secretion in SH-SY5Y cells; (ii) High-dose TBBPA-BHEE (≥20 μM) induces an upregulation of DA secretion, which may be caused by mild cell membrane impairment.

On the other hand, prolonged exposure to pollutants represents a critical factor contributing to cellular damage, and monitoring of this process will be of great significance for health risk assessment. Therefore, we further exposed the cells to TBBPA-BHEE for different time durations (0 h, 12 h, 24 h, 48 h) and employed the cell membrane surface fluorescence monitoring system to track the alterations in biochemical parameters across experimental groups. Fluorescence imaging results in Figure 6B shown that prolonged TBBPA-BHEE exposure led to an upward trend in

the levels of both endogenous targets (Cy5/Cy3 fluorescence ratio for ATP and FAM fluorescence intensity for DA) within the cell membrane surface microenvironment, revealing progressively intensified neurotoxic effects of TBBPA-BHEE. These results demonstrate that the developed tCDNs fluorescence imaging system exhibits the promising potential for sensitive monitoring of multiple biochemical parameters at the cell membrane surface and can provide robust support for health risk assessment of pollutants based on the collected data.

CONCLUSION

In summary, by the design of DNA superstructure, tCDNs, we have successfully developed a cell membrane-anchored dual-target fluorescence monitoring platform. Benefit from the orderly connection of DNA cubes by DNA wireframe structure, the cell membrane anchoring performance of the original monomer nucleic acid framework was significantly enhanced. Under this premise, an in situ monitoring system for ATP and DA was established through the conjugation of fluorescent recognition elements on the tCDNs double-rail scaffold. Using the proposed method, we demonstrate a strong correlation between TBBPA-BHEE exposure scenarios and endogenous biochemical indicator secretion levels, while preliminarily establishing a living cell in situ risk assessment for this emerging organic pollutant. Beyond that, it is also a promising approach to customize the tCDNs architecture by replacing the fluorescent recognition module. We anticipate that this well-designed strategy may serve as a robust tool for risk assessment of environmental pollutants.

ASSOCIATED CONTENT

Supporting Information

The Supporting Information is available free of charge on the ACS Publications website http://pubs.acs.org.

Materials; instruments; experimental details on gel electrophoresis, biostability assay, cytotoxicity assay, cell staining; details of the DNA sequences; supplementary figures presenting schematic diagram of DNA structure, additional electrophoretic characterization diagram, AFM characterization diagram, fluorescence signal intensity and laser confocal microscope results or analysis chart

AUTHOR INFORMATION

Corresponding Author

Zhen Zhang – School of the Environment and Safety Engineering, Jiangsu University, Zhenjiang 212013, China. E-mail: zhangzhen@ujs.edu.cn.

Authors:

Jin Wang – School of the Environment and Safety Engineering, Jiangsu University, Zhenjiang 212013, China.

Zhugen Yang – School of Water, Energy, and Environment, Cranfield University, Cranfield MK43 0AL, UK.

Kun Wang – The School of Chemistry and Chemical Engineering, Jiangsu University, Zhenjiang 212013, China.

Notes

The authors declare no competing financial interest.

ACKNOWLEDGMENTS

This work was supported by the National Natural Science Foundation of China (Grants No. 22176075 and 22476072) and the Jiangsu Collaborative Innovation Center of Technology and Material of Water Treatment.

REFERENCES

1. Su, H.; Guan, G.; Ahmed, R. Z.; Lyu, L.; Li, Z.; Jin, X., TBBPA stimulated cell migration of endometrial cancer via the contribution of NOX-generated ROS in lieu of energy metabolism. *J. Hazard. Mater.* **2020,** *400*, 123204.

2. Yue, R.; Li, X.; Chen, B.; Zhao, J.; He, W.; Yuan, H.; Yuan, X.; Gao, N.; Wu, G.; Jin, H.; Shan, L.; Zhang, W., Astragaloside IV Attenuates Glutamate-Induced Neurotoxicity in PC12 Cells through Raf-MEK-ERK Pathway. *PLOS ONE* **2015,** *10* (5), e0126603.

3. Okeke, E. S.; Feng, W.; Song, C.; Mao, G.; Chen, Y.; Xu, H.; Qian, X.; Luo, M.; Wu, X.; Yang, L., Transcriptomic profiling reveals the neuroendocrine-disrupting effect and toxicity mechanism of TBBPA-DHEE exposure in zebrafish (Danio rerio) during sexual development. *Sci. Total Environ.* **2023,** *858*, 160089.

4. Luo, M.; Wu, Z.; Xu, T.; Ding, Y.; Qian, X.; Okeke, E. S.; Mao, G.; Chen, Y.; Feng, W.; Wu, X., The neurotoxicity and mechanism of TBBPA-DHEE exposure in mature zebrafish (Danio rerio). *Comp. Biochem. Physiol., C: Toxicol. Pharmacol.* **2023,** *267*, 109572.

5. Wu, Q.; Li, G.; Deng, S.; Ouyang, L.; Li, L.; Liu, L.; Luo, N.; Song, X.; He, G.; Gong, C.; Wei, Y., Enhanced antitumor activity and mechanism of biodegradable polymeric micelles-encapsulated chetomin in both transgenic zebrafish and mouse models. *Nanoscale* **2014,** *6* (20), 11940-11952.

6. Okeke, E. S.; Luo, M.; Feng, W.; Zhang, Y.; Mao, G.; Chen, Y.; Zeng, Z.; Qian, X.; Sun, L.; Yang, L.; Wu, X., Transcriptomic profiling and differential analysis revealed the neurodevelopmental toxicity mechanisms of zebrafish (Danio rerio) larvae in response to tetrabromobisphenol A bis(2–hydroxyethyl) ether (TBBPA-DHEE) exposure. *Comp. Biochem. Physiol., C: Toxicol. Pharmacol.* **2022,** *259*, 109382.

7. Włuka, A.; Woźniak, A.; Woźniak, E.; Michałowicz, J., Tetrabromobisphenol A, terabromobisphenol S and other bromophenolic flame retardants cause cytotoxic effects and induce oxidative stress in human peripheral blood mononuclear cells (in vitro study). *Chemosphere* **2020,** *261*, 127705.

8. Eggeling, C.; Ringemann, C.; Medda, R.; Schwarzmann, G.; Sandhoff, K.; Polyakova, S.; Belov, V. N.; Hein, B.; von Middendorff, C.; Schönle, A.; Hell, S. W., Direct observation of the nanoscale dynamics of membrane lipids in a living cell. *Nature* **2009,** *457* (7233), 1159-1162.

9. Worek, F.; Schilha, M.; Neumaier, K.; Aurbek, N.; Wille, T.; Thiermann, H.;

Kehe, K., On-site analysis of acetylcholinesterase and butyrylcholinesterase activity with the ChE check mobile test kit—Determination of reference values and their relevance for diagnosis of exposure to organophosphorus compounds. *Toxicol. Lett.* **2016,** *249*, 22-28.

10. Ekuni, D.; Yamane-Takeuchi, M.; Kataoka, K.; Yokoi, A.; Taniguchi-Tabata, A.; Mizuno, H.; Miyai, H.; Uchida, Y.; Fukuhara, D.; Sugiura, Y.; Tomofuji, T.; Morita, M., Validity of a New Kit Measuring Salivary Lactate Dehydrogenase Level for Screening Gingivitis. *Dis. Markers* **2017,** *2017* (1), 9547956.

11. Tomsič, K.; Seliškar, A.; Lukanc, B.; Nemec Svete, A., Plasma Total Antioxidant Capacity and Activities of Blood Glutathione Peroxidase and Superoxide Dismutase Determined in Healthy Dogs by Using Commercially Available Kits. *Acta Vet.* **2016,** *66* (4), 534-548.

12. Yu, T.; Tang, C.; Zhang, Y.; Zhang, R.; Yan, W., Microfluidics-based digital quantitative PCR for single-cell small RNA quantification†. *Biol. Reprod.* **2017,** *97* (3), 490-496.

13. Kang, C.-C.; Yamauchi, K. A.; Vlassakis, J.; Sinkala, E.; Duncombe, T. A.; Herr, A. E., Single cell–resolution western blotting. *Nat. Protoc.* **2016,** *11* (8), 1508-1530.

14. Kim, H.; Kang, N.; An, K.; Kim, D.; Koo, J.; Kim, M.-S., MRPrimerV: a database of PCR primers for RNA virus detection. *Nucleic Acids Res.* **2017,** *45* (D1), D475-D481.

15. Duan, D.-C.; Liu, J.; Zheng, Y.-L.; Chen, H.; Zhang, X.; Zhang, Y.; Dai, F.; Zhang, S.; Zhou, B., Cellular and Intravital Imaging of NAD(P)H by a Red-Emitting Quinolinium-Based Fluorescent Probe that Features a Shift of Its Product from Mitochondria to the Nucleus. *Anal. Chem.* **2023,** *95* (2), 1335-1342.

16. Yi, D.; Zhao, H.; Zhao, J.; Li, L., Modular Engineering of DNAzyme-Based Sensors for Spatioselective Imaging of Metal Ions in Mitochondria. *J. Am. Chem. Soc.* **2023,** *145* (3), 1678-1685.

17. Liu, C.; Huang, Z.; Jiang, W.; Liu, X.; Li, J.; Han, X.; Tu, H.; Qiu, L.; Tan, W., Programmable pH-Responsive DNA Nanosensors for Imaging Exocytosis and Retrieval of Synaptic Vesicles. *Anal. Chem.* **2020,** *92* (5), 3620-3626.

18. Shi, P.; Wang, Y., Synthetic DNA for Cell-Surface Engineering. *Angewandte Chemie* **2021,** *60* (21), 11580-11591.

19. Schoenit, A.; Cavalcanti-Adam, E. A.; Gopfrich, K., Functionalization of Cellular Membranes with DNA Nanotechnology. *Trends Biotechnol* **2021,** *39* (11),

1208-1220.

20. Liu, J.; Li, W.; Li, R.; Yin, X.; He, S.; Hu, J.; Ruan, S., Programmable DNA Framework Sensors for In Situ Cell-Surface pH Analysis. *Anal. Chem.* **2021,** *93* (36), 12170-12174.

21. Gong, H.; Dai, Q.; Peng, P., Cell-Membrane-Anchored DNA Logic-Gated Nanoassemblies for In Situ Extracellular Bioimaging. *ACS Appl Mater Interfaces* **2022,** *14* (38), 43026-43034.

22. Zeng, S.; Wang, S.; Xie, X.; Yang, S.-h.; Fan, J.-h.; Nie, Z.; Huang, Y.; Wang, H.-h., Live-Cell Imaging of Neurotransmitter Release with a Cell-Surface-Anchored DNA-Nanoprism Fluorescent Sensor. *Anal. Chem.* **2020,** *92* (22), 15194-15201.

23. Ke, G.; Zhu, Z.; Wang, W.; Zou, Y.; Guan, Z.; Jia, S.; Zhang, H.; Wu, X.; Yang, C. J., A Cell-Surface-Anchored Ratiometric Fluorescent Probe for Extracellular pH Sensing. *ACS Appl. Mater. Interfaces* **2014,** *6* (17), 15329-15334.

24. Chidchob, P.; Offenbartl-Stiegert, D.; McCarthy, D.; Luo, X.; Li, J.; Howorka, S.; Sleiman, H. F., Spatial Presentation of Cholesterol Units on a DNA Cube as a Determinant of Membrane Protein-Mimicking Functions. *J. Am. Chem. Soc.* **2019,** *141* (2), 1100-1108.

25. Li, J.; Xun, K.; Pei, K.; Liu, X.; Peng, X.; Du, Y.; Qiu, L.; Tan, W., Cell-Membrane-Anchored DNA Nanoplatform for Programming Cellular Interactions. *J. Am. Chem. Soc.* **2019,** *141* (45), 18013-18020.

26. Li, J.; Xun, K.; Zheng, L.; Peng, X.; Qiu, L.; Tan, W., DNA-Based Dynamic Mimicry of Membrane Proteins for Programming Adaptive Cellular Interactions. *J. Am. Chem. Soc.* **2021,** *143* (12), 4585-4592.

27. Yang, L.; Miao, Y.; Han, D., DNA Nanotechnology on Live Cell Membranes. *CHEM RES CHINESE U* **2020,** *36* (2), 203-210.

28. Xiong, M.; Liu, Q.; Tang, D.; Liu, L.; Kong, G.; Fu, X.; Yang, C.; Lyu, Y.; Meng, H. M.; Ke, G.; Zhang, X. B., "Apollo Program" in Nanoscale: Landing and Exploring Cell-Surface with DNA Nanotechnology. *ACS Appl Bio Mater* **2020,** *3* (5), 2723-2742.

29. Liu, J.; Li, M.; Zuo, X., DNA Nanotechnology-Empowered Live Cell Measurements. *Small* **2022**, e2204711.

30. Guo, Z.; Zhang, L.; Yang, Q.; Peng, R.; Yuan, X.; Xu, L.; Wang, Z.; Chen, F.; Huang, H.; Liu, Q.; Tan, W., Manipulation of Multiple Cell–Cell Interactions by

Tunable DNA Scaffold Networks. *Angew. Chem. Int. Ed.* **2022,** *61* (7), e202111151.

31. Chen, B.; Wang, Y.; Ma, W.; Cheng, H.; Sun, H.; Wang, H.; Huang, J.; He, X.; Wang, K., A Mimosa-Inspired Cell-Surface-Anchored Ratiometric DNA Nanosensor for High-Resolution and Sensitive Response of Target Tumor Extracellular pH. *Anal. Chem.* **2020,** *92* (22), 15104-15111.

32. Qiu, L.; Zhang, T.; Jiang, J.; Wu, C.; Zhu, G.; You, M.; Chen, X.; Zhang, L.; Cui, C.; Yu, R.; Tan, W., Cell Membrane-Anchored Biosensors for Real-Time Monitoring of the Cellular Microenvironment. *J. Am. Chem. Soc.* **2014,** *136* (38), 13090-13093.

33. Zeng, S.; Liu, D.; Li, C.; Yu, F.; Fan, L.; Lei, C.; Huang, Y.; Nie, Z.; Yao, S., Cell-Surface-Anchored Ratiometric DNA Tweezer for Real-Time Monitoring of Extracellular and Apoplastic pH. *Anal. Chem.* **2018,** *90* (22), 13459-13466.

34. Liu, J.; Li, M.; Li, F.; Ge, Z.; Li, Q.; Liu, M.; Shi, J.; Wang, L.; Zuo, X.; Fan, C.; Mao, X., Reconstructing Soma-Soma Synapse-like Vesicular Exocytosis with DNA Origami. *ACS Cent Sci* **2021,** *7* (8), 1400-1407.

35. Ge, Z.; Liu, J.; Guo, L.; Yao, G.; Li, Q.; Wang, L.; Li, J.; Fan, C., Programming Cell–Cell Communications with Engineered Cell Origami Clusters. *J. Am. Chem. Soc.* **2020,** *142* (19), 8800-8808.

36. Akbari, E.; Mollica, M. Y.; Lucas, C. R.; Bushman, S. M.; Patton, R. A.; Shahhosseini, M.; Song, J. W.; Castro, C. E., Engineering Cell Surface Function with DNA Origami. *Adv. Mater.* **2017,** *29* (46), 1703632.

37. Di Virgilio, F.; Sarti, A. C.; Falzoni, S.; De Marchi, E.; Adinolfi, E., Extracellular ATP and P2 purinergic signalling in the tumour microenvironment. *Nat. Rev. Cancer* **2018,** *18* (10), 601-618.

38. Di Virgilio, F.; Adinolfi, E., Extracellular purines, purinergic receptors and tumor growth. *Oncogene* **2017,** *36* (3), 293-303.

39. Gao, T.; Chen, T.; Feng, C.; He, X.; Mu, C.; Anzai, J.-i.; Li, G., Design and fabrication of flexible DNA polymer cocoons to encapsulate live cells. *Nat. Commun.* **2019,** *10* (1), 2946.

40. Liu, Y.; Wijesekara, P.; Kumar, S.; Wang, W.; Ren, X.; Taylor, R. E., The effects of overhang placement and multivalency on cell labeling by DNA origami. *Nanoscale* **2021,** *13* (14), 6819-6828.

41. Büber, E.; Schröder, T.; Scheckenbach, M.; Dass, M.; Franquelim, H. G.; Tinnefeld, P., DNA Origami Curvature Sensors for Nanoparticle and Vesicle Size

Determination with Single-Molecule FRET Readout. *ACS Nano* **2023,** *17* (3), 3088-3097.

42. Wojtowicz, A. K.; Szychowski, K. A.; Kajta, M., PPAR-γ Agonist GW1929 But Not Antagonist GW9662 Reduces TBBPA-Induced Neurotoxicity in Primary Neocortical Cells. *NEUROTOX RES* **2014,** *25* (3), 311-322.

43. Covaci, A.; Harrad, S.; Abdallah, M. A. E.; Ali, N.; Law, R. J.; Herzke, D.; de Wit, C. A., Novel brominated flame retardants: A review of their analysis, environmental fate and behaviour. *Environ. Int.* **2011,** *37* (2), 532-556.

44. Al-Mousa, F.; Michelangeli, F., Some Commonly Used Brominated Flame Retardants Cause Ca^{2+}-ATPase Inhibition, Beta-Amyloid Peptide Release and Apoptosis in SH-SY5Y Neuronal Cells. *PLOS ONE* **2012,** *7* (4), e33059.

45. Liu, Q.; Ren, X.; Long, Y.; Hu, L.; Qu, G.; Zhou, Q.; Jiang, G., The potential neurotoxicity of emerging tetrabromobisphenol A derivatives based on rat pheochromocytoma cells. *Chemosphere* **2016,** *154*, 194-203.

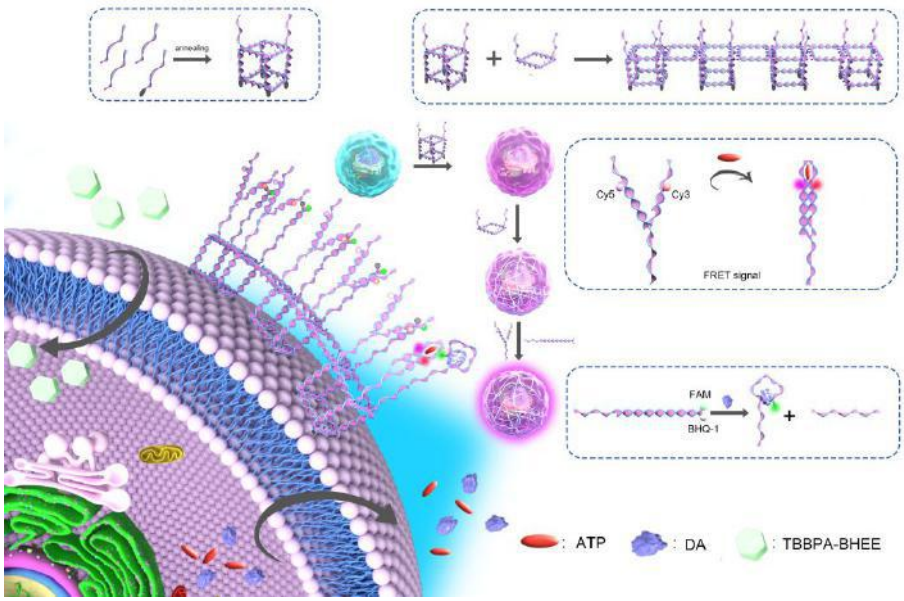

Scheme 1. Schematic illustration of the cell-membrane-anchored tandem cubic DNA nanostructures (tCDNs) nanosensing platform for monitoring the endogenous ATP and DA.

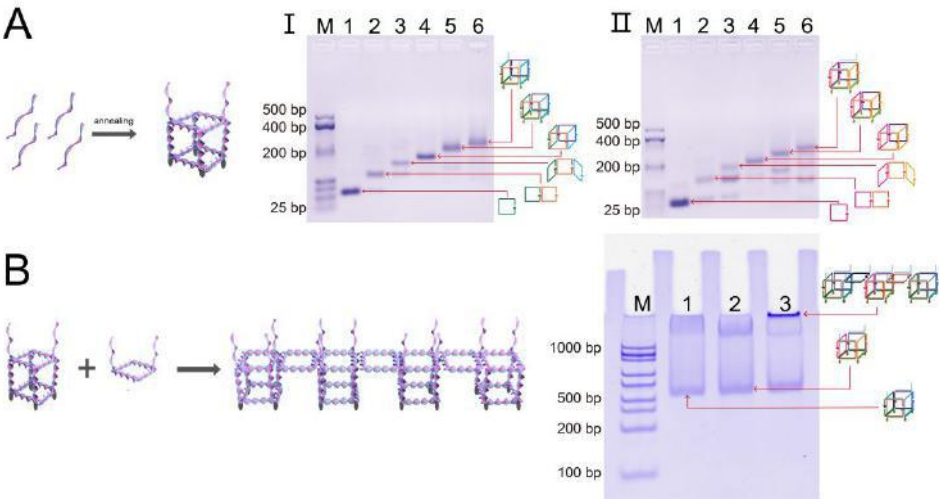

Figure 1. (A) Schematic illustration and self-assembly characterization of the DNA cube framework 1 (Panel Ⅰ, lane M, 25-500 bp marker; lane 1, C1; lane 2, C1+C2; lane 3, C1+C2+C3; lane 4, C1+C2+C3+C4; lane 5, C1+C2+C3+C4+CT20; lane 6, C1+C2+C3+C4+CT20+L50-1+L50-2) and DNA cube framework 2 (Panel Ⅱ, Ⅰ, lane M, 25-500 bp marker; lane 1, C5; lane 2, C5+C6; lane 3, C5+C6+C7; lane 4, C5+C6+C7+C8; lane 5, C5+C6+C7+C8+CT20; lane 6, C5+C6+C7+C8+CT20+L50-1+L50-2) by 2% agarose gel electrophoresis; (B) Schematic illustration and characterization of the self-assembly of the tCDNs framework by 12% native polyacrylamide gel electrophoresis, lane M, 100-1000 bp marker; lane 1, DNA cube framework 1; lane 2, DNA cube framework 2; lane 3, DNA cube framework 1+ DNA cube framework 2+L1+L2.

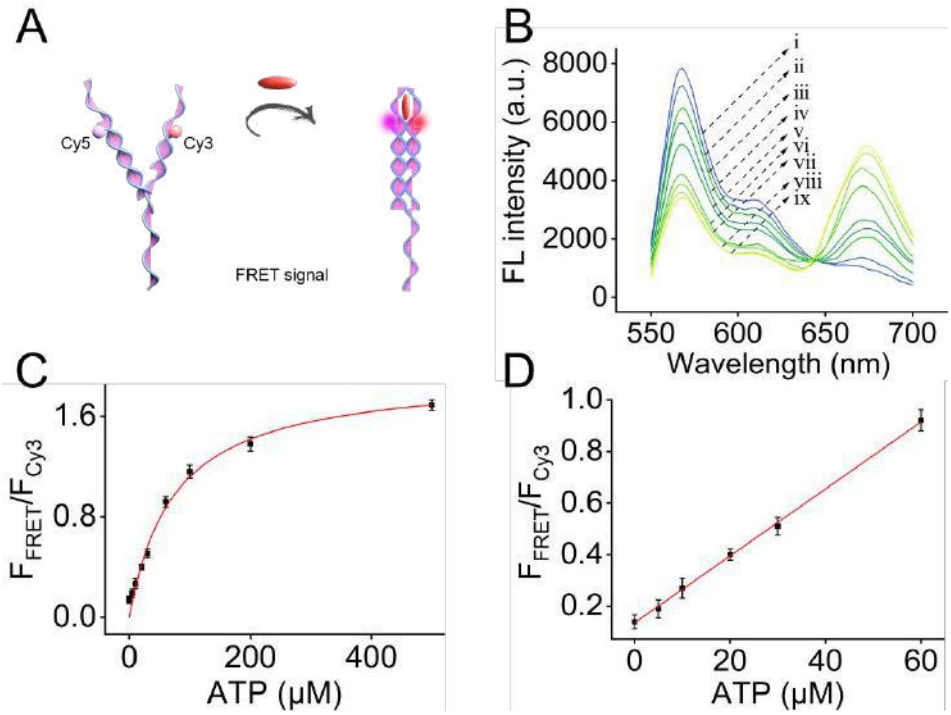

Figure 2. (A) ATP detection mechanism of the DNA aptamer-based nano-tweezers. (B) Fluorescence spectra of the DNA nano-tweezers in response to different concentrations of ATP: (i) 0 μM; (ii) 5 μM; (iii) 10 μM; (iv) 20 μM; (v) 30 μM; (vi) 60 μM; (vii) 100 μM; (viii) 200 μM; (ix) 500 μM. (C) and (D) Linear relationship between Cy5/Cy3 fluorescence ratio and ATP concentrations. (error bars, SD, n = 3).

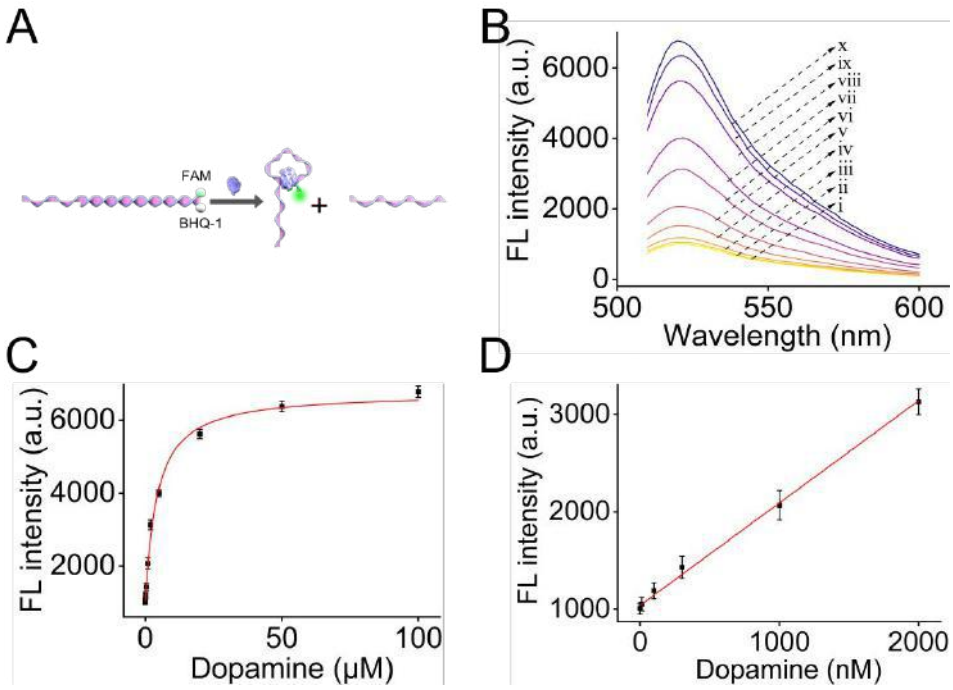

Figure 3. (A) DA detection mechanism of the DA aptamer-based fluorescence recognition elements. (B) Fluorescence spectra of the DNA aptamer-based fluorescence recognition elements in response to different concentrations of DA: (i) 0 μM; (ii) 0.01 μM; (iii) 0.1 μM; (iv) 0.3 μM; (v) 1 μM; (vi) 2 μM; (vii) 5 μM; (viii) 20 μM; (ix) 50 μM; (x) 100 μM. (C) and (D) Linear relationship between FAM fluorescence intensities and DA concentrations. (error bars, SD, n = 3).

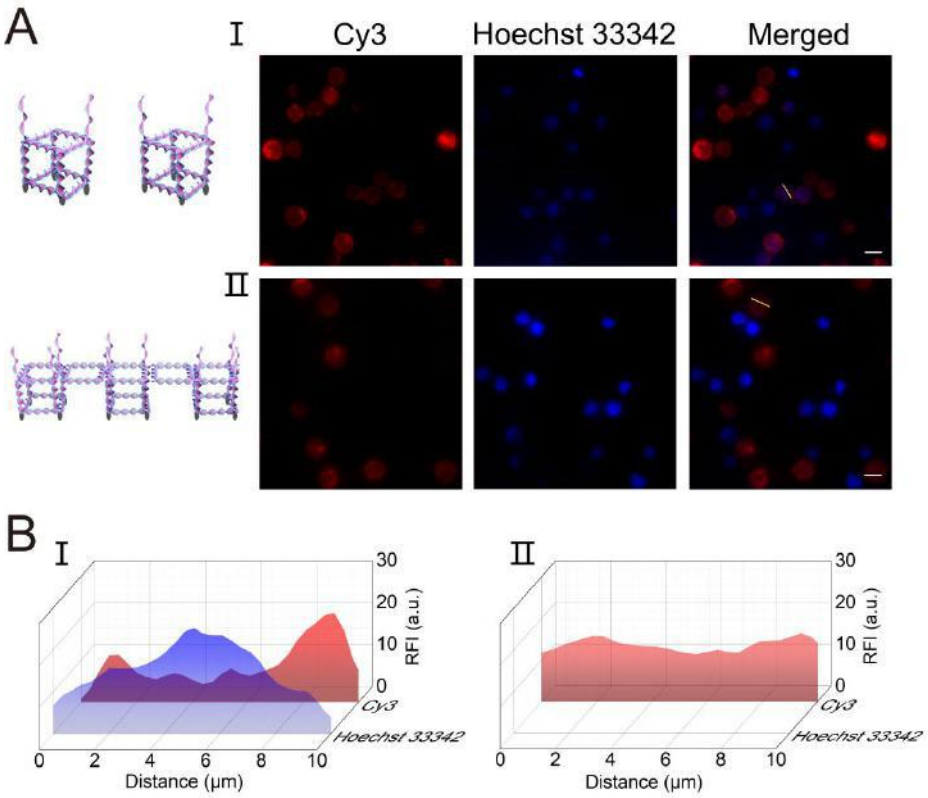

Figure 4. (A) CLSM images of the cell surface-anchored DNA nanostructures. Panel Ⅰ-mixed cell populations of DNA cube monomers-labeled CCRF-CEM cells (red channel, Cy3) and Hoechst 33342-labeled CCRF-CEM cells (blue channel). Panel Ⅱ-mixed cell populations of tCDNs framework-labeled CCRF-CEM cells (red channel, Cy3) and Hoechst 33342-labeled CCRF-CEM cells (blue channel). Scale bar: 10 μm. (B) Cy3 and Hoechst 33342 fluorescence intensity of the linear regions in Panel Ⅰ and Ⅱ merged images.

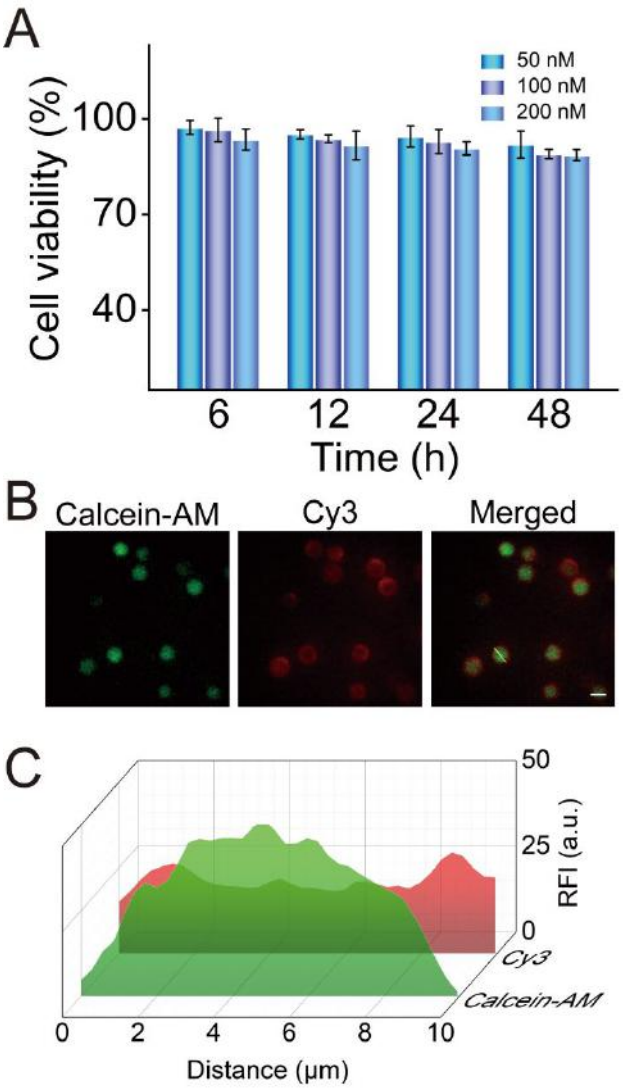

Figure 5. (A) The cell viability investigation of CCRF-CEM cells modified with tCDNs (50, 100, 200 nM) for different times (ranging from 6 to 48 h) at 37 ˚C using CCK-8 kit. (error bars, SD, n = 3). (B) CLSM images of the Calcein-AM (green channel) and tCDNs (red channel, Cy3)-labeled CCRF-CEM cells. Scale bar: 10 μm. (C) Calcein-AM and Cy3 fluorescence intensity of the linear regions in merged images.

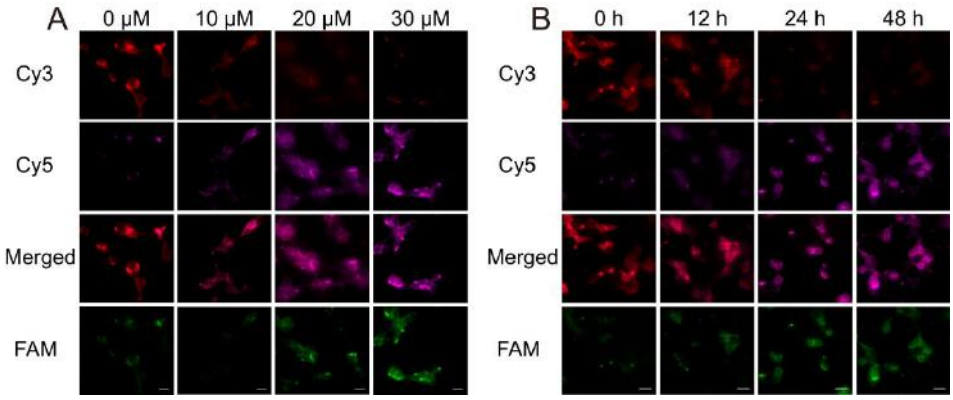

Figure 6. (A) CLSM images of tCDNs nanosensing platform-modified SH-SY5Y cells incubated with different concentrations of TBBPA-BHEE (0, 10, 20, 30 μM) for 24 h. (B) CLSM images of tCDNs nanosensing platform-modified CCRF-CEM cells incubated with 20 μM TBBPA-BHEE for different times (0, 12, 24 and 48 h). Scale bar: 10 μm.

Graphic for Table of Contents (TOC)

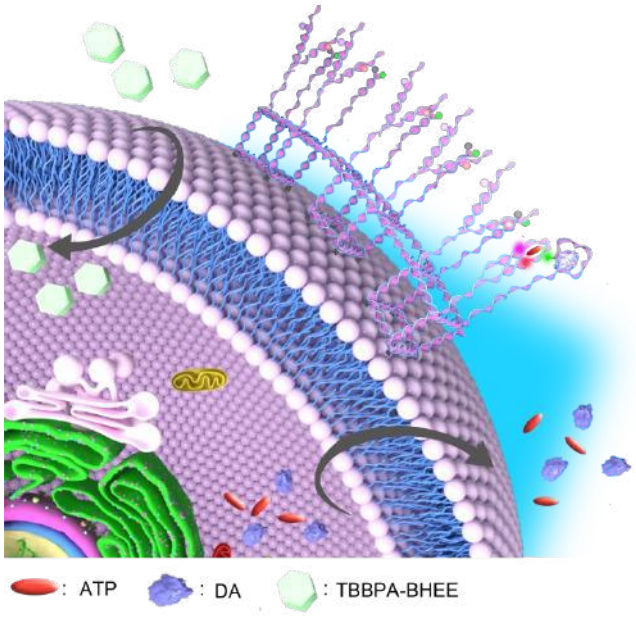

Supporting Information

A Tandem Cubic DNA Nanostructures Cell Membrane Surface Sensing Platform for in situ Monitoring of Multiple Cytotoxicity Related Biomarkers

Jin Wang[1], Zhugen Yang[2], Kun Wang[3], Zhen Zhang[1]*

[1]School of the Environment and Safety Engineering, Jiangsu University, Zhenjiang 212013, China

[2]School of Water, Energy, and Environment, Cranfield University, Cranfield MK43 0AL, UK

[3]The School of Chemistry and Chemical Engineering, Jiangsu University, Zhenjiang 212013, China

*Corresponding author:

Email: zhangzhen@ujs.edu.cn (Zhen Zhang)

This file includes:

1. Table of Contents

2. Supplementary Materials and Methods

3. Table S1

4. Figures S1 to S16

5. References

Table of Contents

Materials **S4**

Instruments **S4**

Gel electrophoresis analysis **S4**

Biostability assay of tCDNs **S5**

Cytotoxicity assay **S5**

Cell staining **S5**

Table S1. Details of the DNA sequences **S7**

Figure S1. Schematic diagram of the two-dimensional unfolding of DNA cubes and their connection with auxiliary DNA strands **S8**

Figure S2. Fluorescence excitation (Ex) and emission (Em) spectra of Cy3 ..... **S9**

Figure S3. Characterization of the DNA cube backbone oligonucleotides by 12% native polyacrylamide gel electrophoresis **S10**

Figure S4. Characterization of the auxiliary DNA oligonucleotides by 12% native polyacrylamide gel electrophoresis **S11**

Figure S5. AFM characterization of the mixed DNA cubes 1/2 and and their assembled tCDNs **S12**

Figure S6. Stability investigation of the tCDNs fireworks in different solutions **S13**

Figure S7. Schematic diagram and self-assembly characterization of ATP aptamer-based nano-tweezers **S14**

Figure S8. Schematic diagram and self-assembly characterization of the DA aptamer-based fluorescence recognition elements **S15**

Figure S9. Fluorescence response of the tCDNs fluorescence system to ATP, GTP, UTP, CTP and the mixture. **S16**

Figure S10. Fluorescence spectral responses of the DA aptamer-based fluorescence recognition elements **S17**

Figure S11. Fluorescence response of the tCDNs fluorescence system to DA, NP, 5-HT, Tyt, AA, Glu and the mixture **S18**

Figure S12. Cell surface anchoring of the tCDNs **S19**

Figure S13. CLSM images of the CCRF-CEM cells labeled with Cy3-DNA cubes, Cy3-tCDNs and Hoechst 33342 ..... **S20**

Figure S14. Comparison of cell membrane surface anchoring maintenance time **S21**

Figure S15. CLSM images and fluorescence intensities of tCDNs nanosensing platform-modified SH-SY5Y cells incubated with different concentrations of ATP or DA **S22**

Figure S16. The orthogonal fluorescence triggering validation of target analytes and the fluorescence response validation of mismatched aptamer sequences for the tCDNs nanosensing platform **S23**

Supplementary Materials and Methods

Materials. All HPLC purified standard and modified DNA oligonucleotides (**Table S1**), Cell Counting Kit-8, trypsin-EDTA (TE) buffer and phosphate-buffered saline (PBS, 1×, pH=7.4) were commercially supplied by Sangon Biotechnology Co., Ltd (Shanghai, China). Fetal bovine serum (FBS) was obtained from Zhejiang Tianhang Biotechnology Co.,Ltd. 1640, DMEM and MEM/F12 medium were purchased from Solarbio Science & Technology Co., Ltd. CCRF-CEM (Human T-cell ALL) and SH-SY5Y cell lines were obtained from Wuhan Pricella Biotechnology Co., Ltd. Cell plasma membrane staining kit with DiO (green fluorescence), Hoechst 33342 staining solution for live cells (100×) and Calcein-AM staining solution (100×) were purchased from Beyotime Biotechnology Co., Ltd. Ultrapure water was obtained through a Millipore Milli-Q water purification system (Milli-Q, 18 MΩ·cm resistivity at 25 C, Merck Millipore).

Instruments. All fluorescence measurements were carried on a BioTek Synergy H4 multi-mode microplate reader (BioTek Instruments, Inc., VT, USA). The number of cells was measured with a TC10 automated cell counter (Biorad, USA). Confocal fluorescence imaging of cells was performed on a Leica TCS SP5 II Laser confocal laser scanning microscopy (CLSM, Leica Microsystems, Inc., Wetzlar, Germany). All the CLSM images were digitized and analyzed with ImageJ software.

Gel electrophoresis analysis. Agarose gel (2%) electrophoresis (AGE) and native polyacrylamide gel (12%) electrophoresis (native PAGE) were used to verify the self-assembly of tCDNs and DNA aptamer nanosensing elements. AGE was conducted at a constant potential of 110 V in 1× TBE buffer. The electrophoresis run time was determined by the indicators in the loading buffer and was approximately 40 minutes. Native PAGE was prepared with 4 mL of ultrapure water, 1.6 mL of 10× TBE buffer, 2.4 mL of 40% acryl-bis, 56 μL of 10% APS, and 8 μL of TEMED. Similarly, native PAGE was run at 110 V for about 30 min (4 °C) in 1× TBE buffer and stained by Super GelRed nucleic acid dye. After electrophoresis, all the pictures were obtained with a

Gel Imaging System.

Biostability assay of tCDNs. For endonuclease resistance verification, the prepared tCDNs were added to PBS buffer containing 0.5 U/mL DNase I and incubated at 37 ℃ for different time (2, 4, 6, 8 and 10 h). Similarly, for the biostability test under serum conditions, tCDNs were added to PBS buffer containing 10% FBS and incubated at 37 ℃. Furthermore, the adaptability of tCDNs to different acidities was tested using 5 groups of solutions with different pH values (5-9) at 37 ℃ for 8 hours. The final products of all above experiments were used for native PAGE gel electrophoresis characterization without further treatment.

Cytotoxicity assay. Cytotoxicity of tCDNs was estimated in CCRF-CEM cells by Cell Counting Kit-8 (CCK-8). First, SH-SY5Y cells were seeded into 96-well plates (2×10^4 cell/well) to a total volume of 200 μL/well and cultured at 37 °C for 24 h. Then, the cells were incubated with 100 μL MEM/F12 medium containing TDNs (50, 100, 200 nM) for different times (6, 12, 24, 48 h). As control groups, the SH-SY5Y cells were treated with MEM/F12 medium and incubated for the same time to eliminate the background interference of cell proliferation. After being washed three times by PBS solution and replaced with fresh MEM/F12 medium, each well was added with 10 μL of CCK-8 solution. The absorbance (450 nm) was measured by multi-mode microplate reader after 1 h of reaction.

Cell staining. For DiO dye, an appropriate volume of 1:200 DiO dilution was used to resuspend CCRF-CEM cells at a density of 1×10^5 cells/mL. The cells were then incubated for 10 minutes and centrifuged to remove the staining solution. Following three washes with PBS buffer, the cells were resuspended in fresh 1640 medium. For Calcein-AM dye, 1×10^5 CCRF-CEM cells are washed 3 times with PBS and then added to the pre-warmed Calcein-AM working solution (1 μM) and incubated at 37 °C for 20 minutes. After centrifugation to remove the staining solution, cells are resuspended in fresh 1640 medium. For Hoechst 33342 staining, CCRF-CEM cells at a density of 1×10^5 cells/mL were incubated with Hoechst 33342 staining solution at 37°C for 30

minutes. Then, washed 3 times with PBS buffer and the CCRF-CEM cells were resuspended in fresh 1640 medium.

Table S1. Details of the DNA sequences.

Oligo	Sequence (5'-3')
C1 (C5)	TCGCTGAGTATTTTATCTCACGAAGCATACGAGCTTTTGCAAGTG TGGGCACGCACACTTTTGTAACCGCGACTGCGAGAGTTTTTCACA AATCTG
C2	CTATCGGTAGTTTTGCCTAGAGGATCCGAGTTCGTTTTTACTCAGC GACAGATTTGTGTTTTGTAACCGCGACTGCGAGAGTTTTTCAACT AGCGG
C3 (C7)	CACTGGTCAGTTTTGAGCAGTTGACCATATAGGATTTTCTACCGA TAGCCGCTAGTTGTTTTGTAACCGCGACTGCGAGAGTTTTTGGTTT GCTGA
C4	CCACACTTGCTTTTGTAGCTTGCCCATAATTTGGTTTTCTGACCAG TGTCAGCAAACCTTTTGTAACCGCGACTGCGAGAGTTTTTGTGTG CGTGC
C6	CTATCGGTAGTTTTGAGATACACAAGGTGAGCACTTTTTACTCAG CGACAGATTTGTGTTTTGTAACCGCGACTGCGAGAGTTTTTCAAC TAGCGG
C8	CCACACTTGCTTTTGGAAAGCTGATCAGTGGTCATTTTCTGACCA GTGTCAGCAAACCTTTTGTAACCGCGACTGCGAGAGTTTTTGTGT GCGTGC
CT20	ACTCTCGCAGTCGCGGTTACTTTTT-cholesterol
L1	TCCTCTAGGCTTTTGAGCAGTTGACCATATAGGATTTTTGACCACT GATCAGCTTTCCTTTTATCTCACGAAGCATACGAGCTTTTCGAACT CGGA
L2	TGTGTATCTCTTTTGAGCAGTTGACCATATAGGATTTTCCAAATTA TGGGCAAGCTACTTTTATCTCACGAAGCATACGAGCTTTTGTGCT CACCT
L50-1	GCTCGTATGCTTCGTGAGATTTTTTCATGGGCTCATGCGAGGCTGT ATGT
L50-2	TCCTATATGGTCAACTGCTCTTTTTCGATAATAGTGGTATCGGACG GCTC
LF	Cy3-TTTTTACATACAGCCTCGCATGAGCCCATG
A1	TGCGGAGGAAGGTTACATTTTACGCCTGGTGCCTTTTTACATACA GCCTCGCATGAGCCCATG
Mismatched A1	TATTAAGGCCTGTTACATTTTACGCCTGGTGCCTTTTTACATACAG CCTCGCATGAGCCCATG
A2	CCGACCGCAGGATCCTATAAACCTGGGGGAGTAT
Mismatched A2	CCGACCGCAGGATCCTATAAACCTGTCCACCATT
A3	Cy3-TTATAGGATCCTGCGGTCGGAGGCACCAGGCGTAAAATGTA-Cy5
DP	FAM-CTCTCGGGACGACGCCAGTTTGAAGGTTCGTTCGCAGGTGTGGAG TGACGTCGTCCCTTTTTGAGCCGTCCGATACCACTATTATCG
CP	CGTCGTCCCGAGAG-BHQ1
Mismatched DP	FAM-CTCTCGGGACGACGCCAGAACGCTAATACGTACCTCGATGACTTG CAACGTCGTCCCTTTTTGAGCCGTCCGATACCACTATTATCG

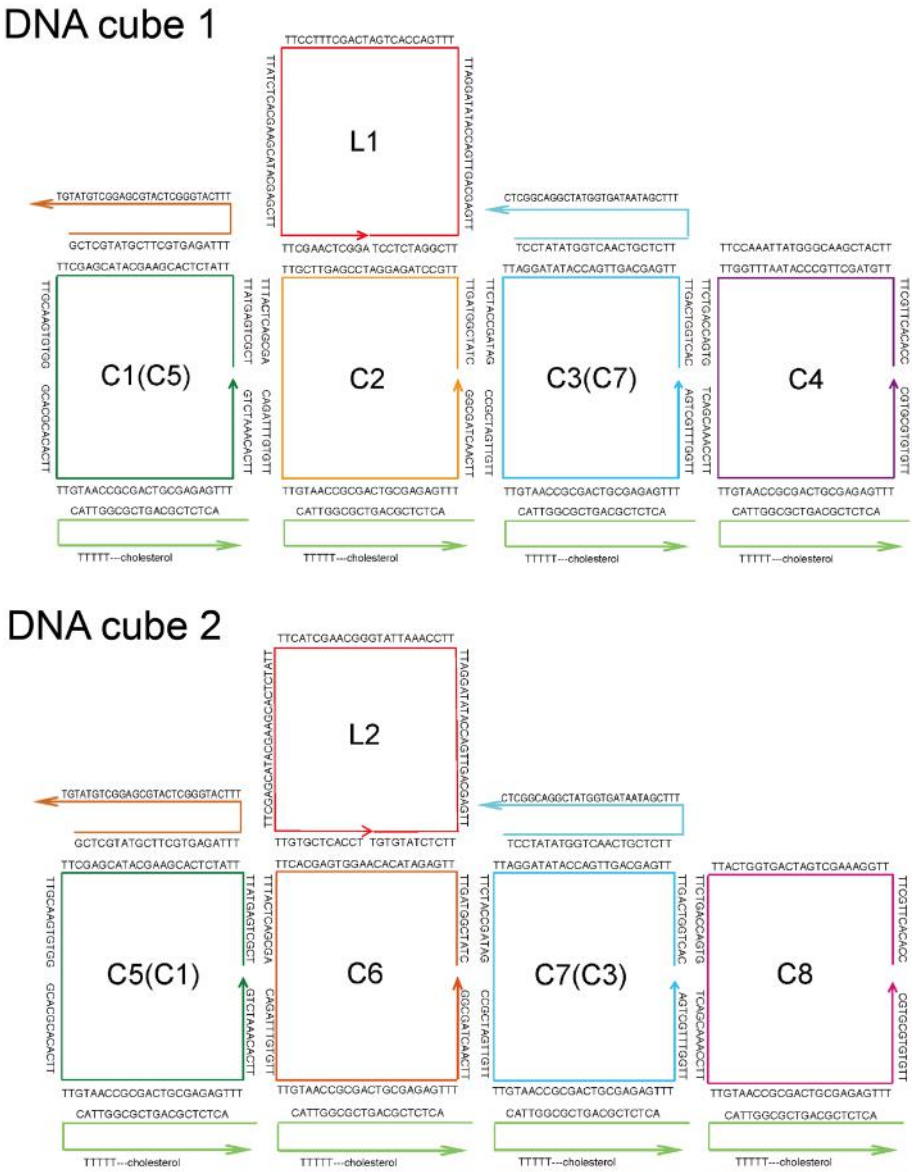

Figure S1. Schematic diagram of the two-dimensional unfolding of DNA cube 1(C1, C2, C3, C4) and cube (C5, C6, C7, C8) their connection with auxiliary DNA strands (L1, L2, L50-1, L50-2 and CT20). All the arrows point to the 3' end of the DNA sequences.

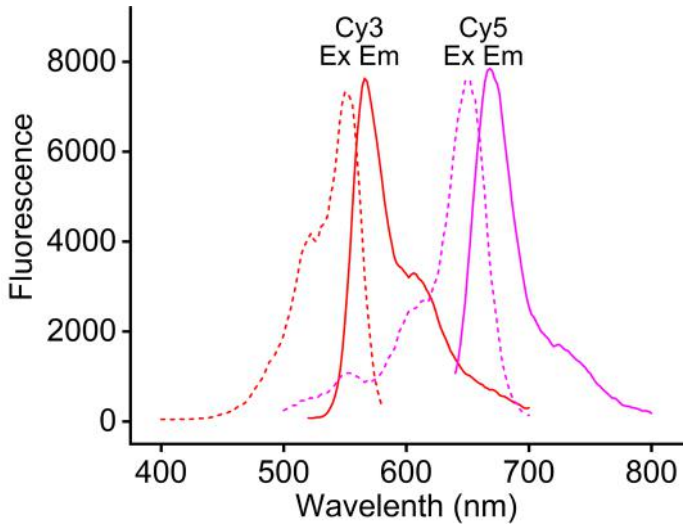

Figure S2. Fluorescence excitation (Ex) and emission (Em) spectra of Cy3(Ex = 550 nm, Em = 570 nm) and Cy5 (Ex = 650 nm, Em = 670 nm) measured by 100 nM A3.

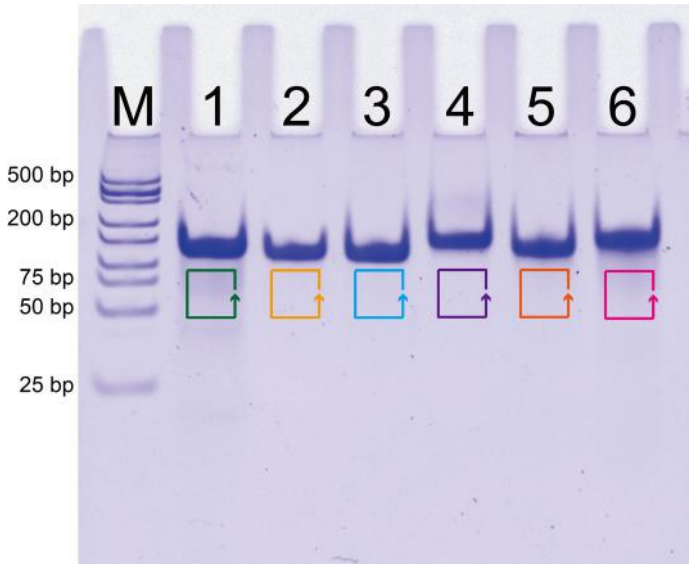

Figure S3. Characterization of the DNA cube backbone oligonucleotides by 12% native polyacrylamide gel electrophoresis. Lane M, 25-500 bp marker; lane 1, C1 (C5); lane 2, C2; lane 3, C3 (C7); lane 4, C4; lane 5, C6; lane 6, C8.

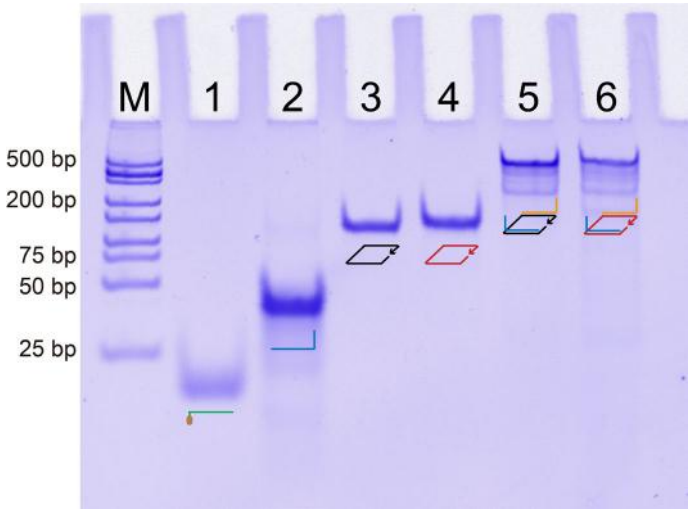

Figure S4. Characterization of the auxiliary DNA oligonucleotides by 12% native polyacrylamide gel electrophoresis. Lane M, 25-500 bp marker; lane 1, CT20; lane 2, L50-1; lane 3, L1; lane 4, L2; lane 5, L1 + L50-1 + L50-2; lane 6, L2 + L50-1 + L50-2.

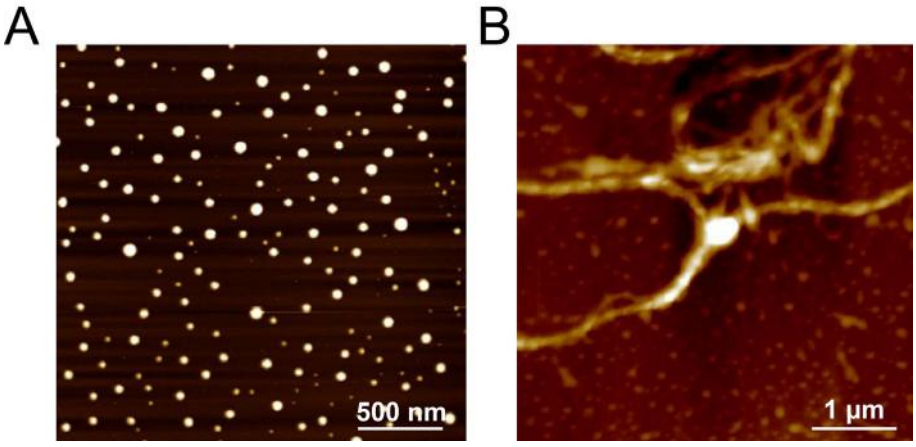

Figure S5. AFM characterization of the mixed DNA cubes 1/2 (A) and and their assembled tCDNs (B).

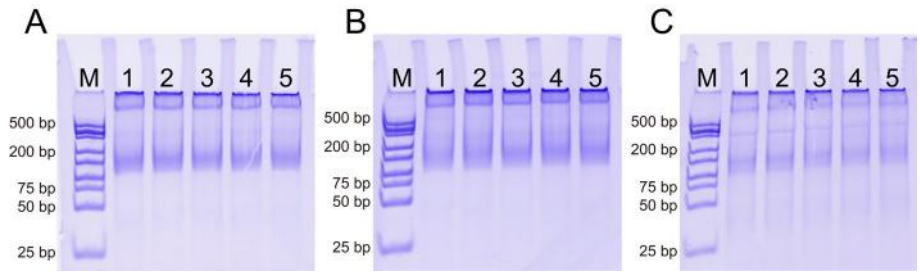

Figure S6. (A) Stability investigation of the tCDNs superstructure by incubation with 0.5 U/mL DNase I for different times. From Lanes 1 to 5: 2, 4, 6, 8, 10 hours; lane M, 25-500 bp marker. (B) Stability investigation of the tCDNs fireworks by incubation with 10% FBS for different times. From Lanes 1 to 5: 2, 4, 6, 8, 10 hours; lane M, 25-500 bp marker. (C) Stability investigation of the tCDNs fireworks at different pH values. From Lanes 1 to 5: pH 5, 6, 7, 8, 9; lane M, 25-500 bp marker. All experimental results were presented using 12% native polyacrylamide gel electrophoresis.

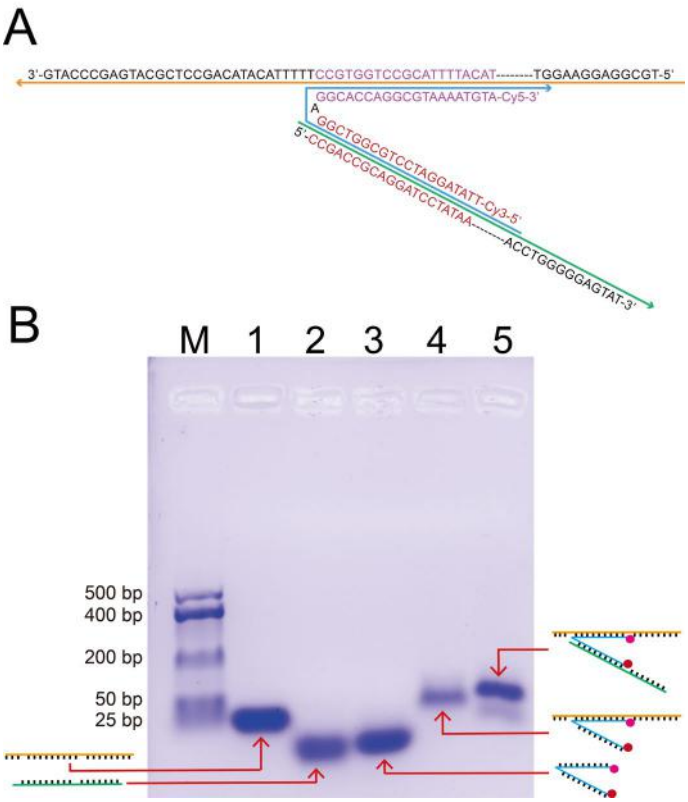

Figure S7. (A) Schematic diagram of the ATP aptamer-based nano-tweezers. (B) Self-assembly characterization of the ATP aptamer-based nano-tweezers by 2% agarose gel electrophoresis. Lane M, 25-500 bp marker; lane 1, A1; lane 2, A2; lane 3, A3; lane 4, A1 + A3; lane 5, A1 + A2 + A3.

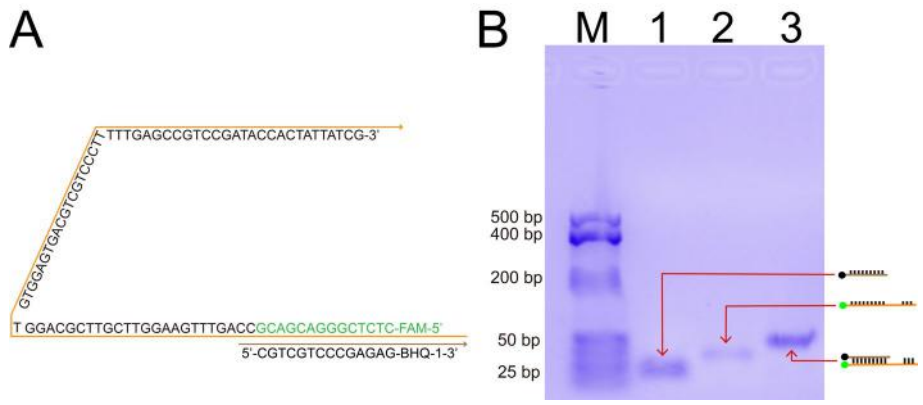

Figure S8. (A) Schematic diagram of the DA aptamer-based fluorescence recognition elements. (B) Self-assembly characterization of the DA aptamer-based fluorescence recognition elements by 2% agarose gel electrophoresis. Lane M, 25-500 bp marker; lane 1, CP; lane 2, DP; lane 3, DP + CP.

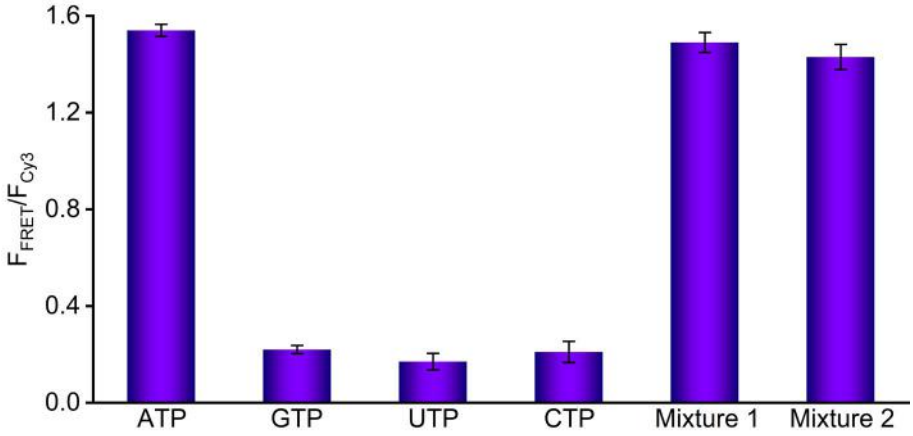

Figure S9. Fluorescence response of the tCDNs fluorescence system to ATP, GTP, UTP, CTP and the mixture. Mixture 1: ddH_2O containing ATP, GTP, UTP and CTP; Mixture 2: ddH_2O containing ATP, GTP, UTP, CTP and 10% FBS. (error bars, SD, n = 3).

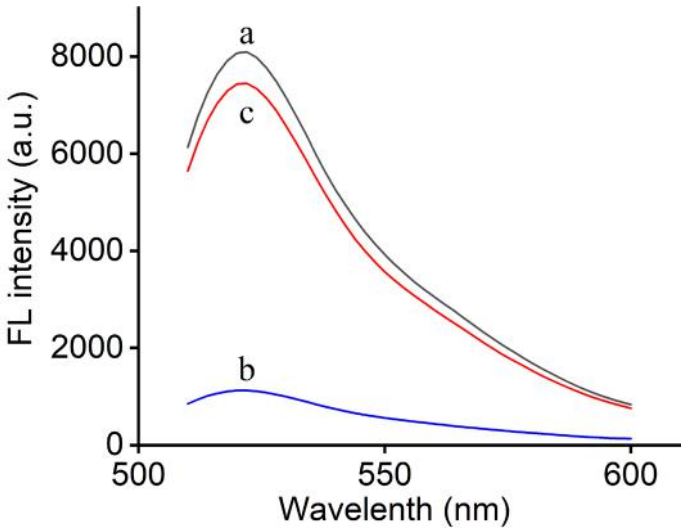

Figure S10. FAM fluorescence spectral responses of the DA aptamer-based fluorescence recognition elements: (a) 100 nM DP; (b) 100 nM DP + 100 nM CP; (c) 100 nM DP + 100 nM CP co-incubated with 100 nM DA.

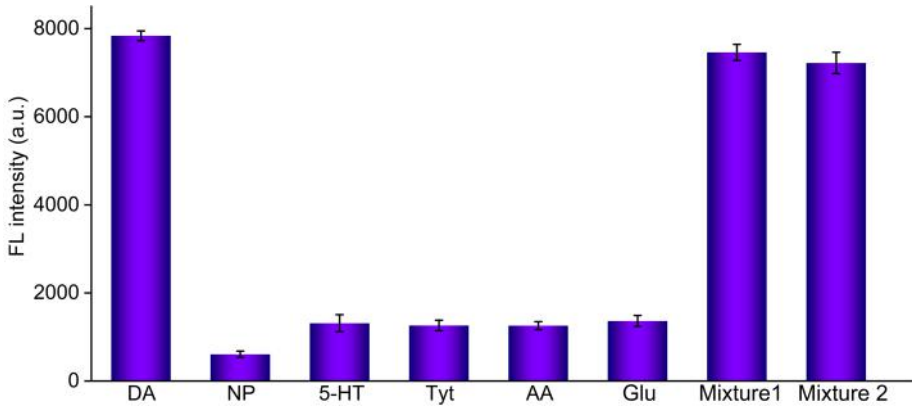

Figure S11. Fluorescence response of the tCDNs fluorescence system to DA, NP, 5-HT, Tyt, AA, Glu and the mixture. Mixture 1: ddH_2O containing DA, NP, 5-HT, Tyt, AA and Glu; Mixture 2: ddH_2O containing DA, NP, 5-HT, Tyt, AA, Glu and 10% FBS. (error bars, SD, n = 3).

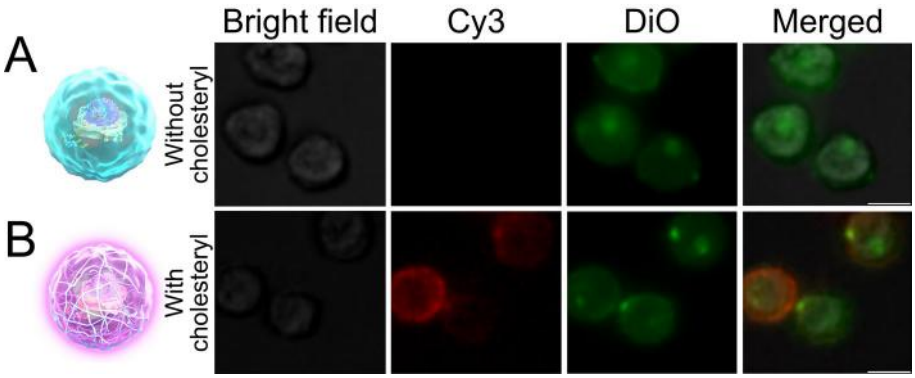

Figure S12. Cell surface anchoring of the tCDNs. (A) Schematic illustration and CLSM images of CCRF-CEM cells after incubation with the no cholesterol-modified short strand (CT20); (B) Schematic illustration and confocal images of CCRF-CEM cells after incubation with the CT20. Then, the cell membrane was stained with DiO. Scale bar: 10 μm.

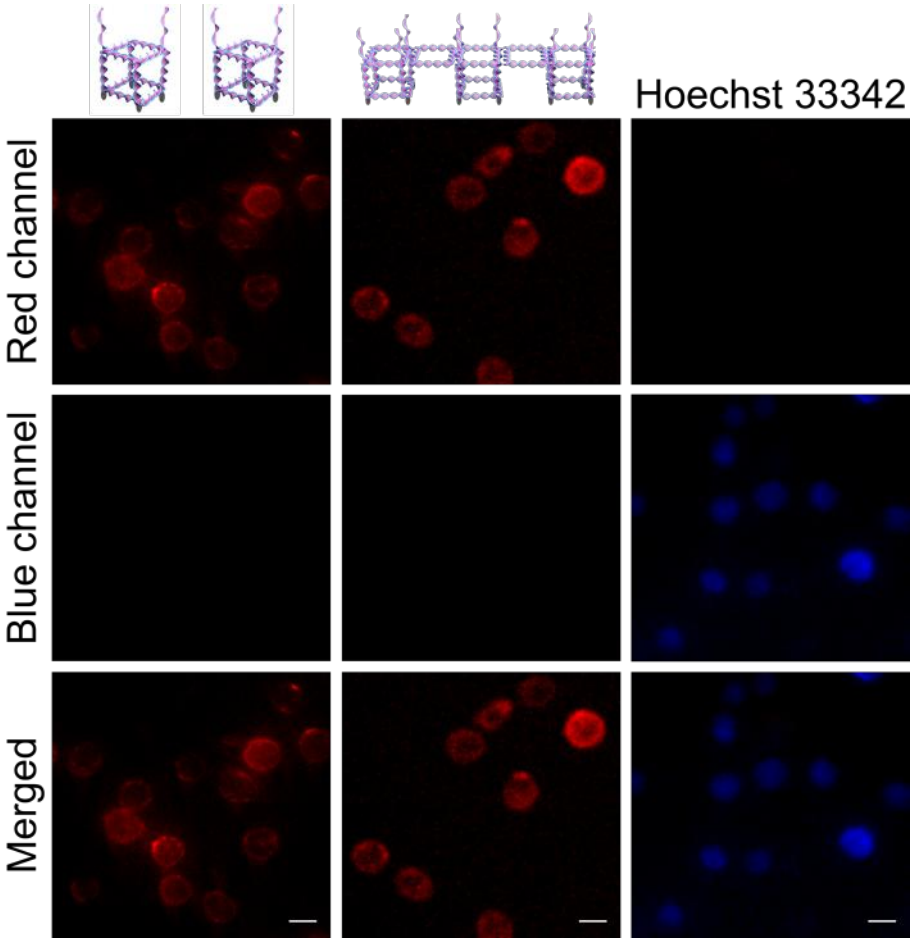

Figure S13. CLSM images of the CCRF-CEM cells incubation with Cy3 labeled-DNA cubes (red channel), Cy3 labeled-tCDNs (red channel), and Hoechst 33342 (blue channel), respectively. Scale bar: 10 μm.

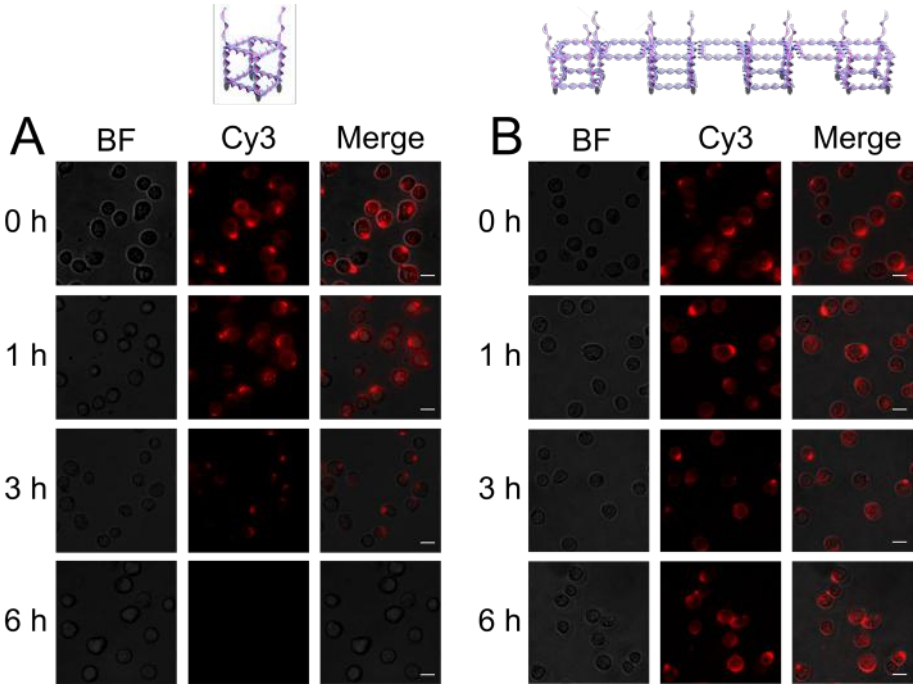

Figure S14. Comparison of cell membrane surface anchoring maintenance time. (A) CCRF-CEM cells were modified with monomeric DNA cubes and maintained for 0, 1, 3, 6 hours in serum-free 1640 medium. (B) CCRF-CEM cells were modified with tCDNs architecture and maintained for 0, 1, 3, 6 hours in serum-free 1640 medium. Scale bar: 10 μm.

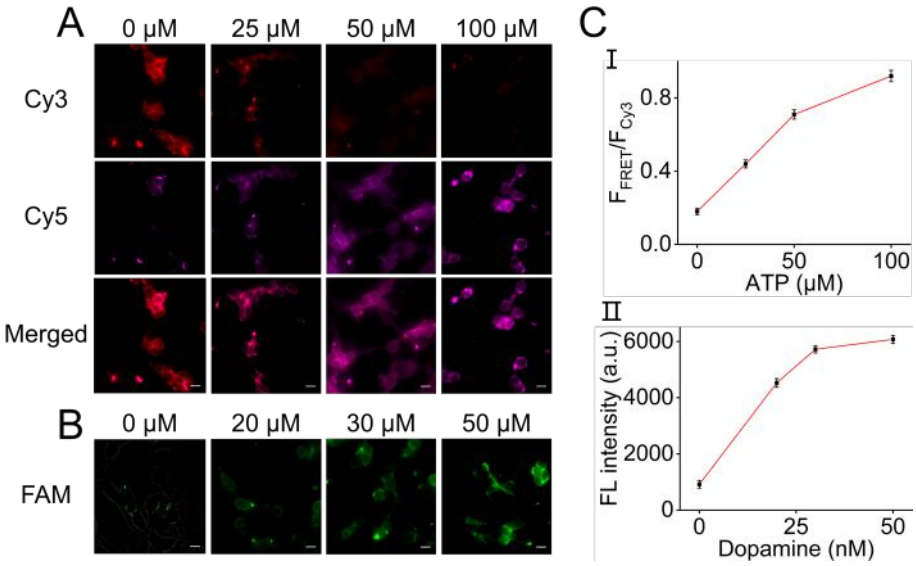

Figure S15. (A) CLSM images of tCDNs nanosensing platform-modified SH-SY5Y cells incubated with different concentrations of ATP (0, 25, 50 and 100 μM). (B) CLSM images of tCDNs nanosensing platform-modified SH-SY5Y cells incubated with different concentrations of DA (0, 20, 30 and 50 μM). (C) Panel I: relationship between Cy5/Cy3 fluorescence ratio and ATP concentrations. Panel II: relationship between FAM fluorescence intensities and DA concentrations. Scale bar: 10 μm. (error bars, SD, n = 3).

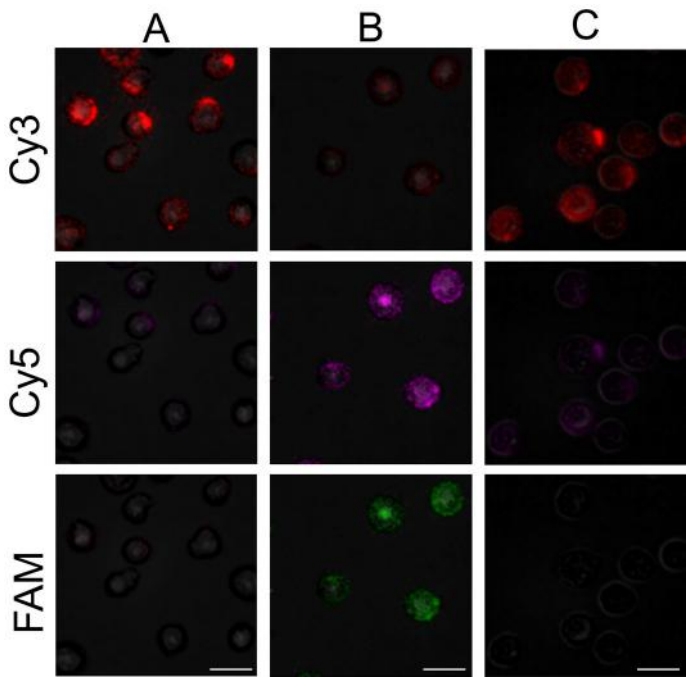

Figure S16. The orthogonal fluorescence triggering validation of target analytes and the fluorescence response validation of mismatched aptamer sequences for the tCDNs nanosensing platform. (A) CLSM images of tCDNs nanosensing platform-modified CCRF-CEM cells incubated with no ATP or DA. (B) CLSM images of tCDNs nanosensing platform-modified CCRF-CEM cells incubated with 100 μM ATP and 50 μM DA. (C) CLSM images of tCDNs nanosensing platform (use mismatched aptamer sequences) -modified CCRF-CEM cells incubated with 100 μM ATP and 50 μM DA. Scale bar: 20 μm.

https://dspace.org/

A tandem cubic DNA nanostructures cell membrane surface sensing platform for in situ monitoring of multiple cytotoxicity-related biomarkers

Wang, Jin; Yang, Zhugen; Wang, Kun; Zhang, Zhen

2025-10-28
American Chemical Society (ACS)
https://doi.org/10.1021/acs.analchem.5c04753
Wang J, Yang Z, Wang K, Zhang Z. (2025) A tandem cubic DNA nanostructures cell membrane surface sensing platform for in situ monitoring of multiple cytotoxicity-related biomarkers. Analytical Chemistry, Volume 97, Issue 42, October 2025, pp. 23496-23504

Downloaded from a DSpace repository. https://dspace.org/